Validation of ATI SAR ocean and sea ice surface velocity derived from TanDEM-X and coastal radar data, near Barrow, Alaska

Master Thesis
M.Sc. Program for Polar and Marine Science POMOR

Saint Petersburg State University / Hamburg University
by
Eduard Khachatrian
Saint Petersburg / Hamburg, 2017

Contents

List of Figures

List of Tables

VALIDATION OF ATI SAR OCEAN AND SEA ICE SURFACE VELOCITY DERIVED FROM TANDEM-X AND COASTAL RADAR DATA, NEAR BARROW, ALASKA

Eduard Khachatrian

Master Program for Polar and Marine Sciences POMOR / 022000 Ecology and environmental management

Supervisors:

Prof. Dr. Lars Kaleschke, Hamburg University, Remote Sensing and Assimilation, Hamburg, Germany

Dr. Vladimir Volkov, Nansen International Environmental and Remote Sensing Centre (NIERSC), Saint-Petersburg, Russia

Considerable changes of sea ice cover that have occurred in the new millennium, inspired scientists to invent new algorithms for classification of ice formations and analysis of sea ice drift. The reliable measurement of sea ice drift became possible in the late 1970s in consequence of satellite appearance and since that moment scientists have been inventing higher-end technologies and methods to measure sea ice characteristics.

Interferometry SAR method which was used in this work differs from other methods of sea ice drift calculation and fast ice detection. In addition, up until this work, this method has been used for other purposes, including topographic measurements and calculation of ocean currents. But in our work, it was used to measure the velocity and direction of sea ice drift and the separation of fast ice from drift ice zones. Applications of InSAR techniques for the drift ice are possible only in a single-pass mode because of temporal decorrelation. An important factor of the InSAR method is that the interferometric phase difference, which is readily provided in the data as an interferogram, is linearly related to the radial velocity. However, this method can not be called accurate in terms of sea ice velocity calculation, because the interferometric phase difference contains several types of information, such as topographic, motion of surface and noise, which could produce some errors in the interferogram. On the other hand, if to compare the InSAR method with

other automatic methods of sea ice drift calculation, it can be said that the main difference and at the same time the primary advantage is that a pair of images is obtained almost simultaneously (less than a second), this in turn allows to conduct the operational sea ice monitoring. The results demonstrate the possibility of fast ice detection, which would be incredibly useful for the scientific and commercial purposes.

For the data analysis in this work, several datasets from different satellite systems and coastal radar were used. The main satellite images were obtained from the TanDEM-X mission, which provides high resolution images. For this study was selected the test site area near Barrow, Alaska, which is the northernmost point of the United States of America. This work will show how suitable this method is in comparison with other automatic methods of fast ice detection and sea ice drift calculation.

ВАЛИДАЦИЯ СКОРОСТИ ПОВЕРХНОСТНЫХ ТЕЧЕНИЙ И ДРЕЙФА МОРСКОГО ЛЬДА, ПОЛУЧЕННЫХ НА ОСНОВЕ ДАННЫХ ПРОДОЛЬНОЙ ИНТЕРФЕРОМЕТРИИ РАДАРА С СИНТЕЗИРОВАННОЙ АПЕРТУРОЙ TANDEM-X И ДАННЫХ ПРИБРЕЖНОГО РАДАРА, ДЛЯ РАЙОНА ВБЛИЗИ МЫСА БАРРОУ, АЛЯСКА

Хачатрян Эдуард

Магистерская программа «Полярные и морские исследования» («ПОМОР») / 022000 «Экология и природопользование»

Выпускная квалификационная работа магистра

Научные руководители:
Профессор Калешке Л., Гамбургский университет, Дистанционное зондирование и Ассимиляция, Гамбург, Германия
Д-р Волков В., Международный центр по окружающей среде и дистанционному зондироанию имени Нансена, Санкт-Петербург, Россия

Значительные изменения морского ледяного покрова, произошедшие в новом тысячелетии, вдохновили ученых на разработку новых алгоритмов классификации ледяных образований и анализа дрейфа морского льда. Достоверные измерения дрейфа морского льда стали возможны с 1970-х годов с появлением спутниковых технологий. С тех пор, ученые начали изобретать все более передовые технологии и методы для измерения различных характеристик морского льда.

Интерферометрический РСА (ИнРСА) метод, использованный в данной работе, отличается от других методов расчета дрейфа льда и обнаружения припайных зон. Ранее эта технология применялась для других целей, например, для топографических измерений или вычисления скорости морских течений. Однако в данной работе интерферометрический РСА метод используется для измерения скорости и направления дрейфа морского льда, а также для разделения зон неподвижного и дрейфующего морского льда. Важной особенностью применения ИнРСА метода является то, что интерферометрическая разность

фаз, представленная в данных в виде интерферограммы, линейно связана с радиальной скоростью. Кроме того, использование методов ИнРСА, для наблюдений за дрейфующим льдом, возможно только в однопроходном режиме. С точки зрения вычисления скорости морского льда эту технологию нельзя назвать предельно точной, так как интерферометрическая разность фаз содержит несколько типов информации – топографию, движение поверхности, шум, которые в свою очередь могут привести к ошибкам в интерферограмме. С другой стороны, главным отличием и в то же время основным преимуществом данного метода является то, что пара изображений получается почти одновременно, с дискретностью меньше секунды, это позволяет проводить оперативный мониторинг морского льда. Результаты ярко демонстрируют возможность обнаружения припайных зон, что может быть невероятно полезным для научных и коммерческих целей.

Для анализа было использовано несколько типов данных, полученных с различных спутниковых систем и прибрежного радара. Основные спутниковые изображения были получены со спутниковой миссии TanDEM-X, которая обеспечивает изображения с высоким разрешением. Для исследования была выбрана область вблизи Барроу, Аляска – самая северная точка США. Данная работа раскрывает основные преимущества и недостатки ИнРСА метода по сравнению с другими автоматическими методами обнаружения припайных зон и расчета полей дрейфа морского льда.

List of used abbreviations

1. AT, ATI - Along-Track, Along-Track Interferometry
2. CoSSC - Coregistered Single look Slant range Complex
3. DEM - Digital Elevation Measurement
4. DLR - German Aerospace Center
5. DRA - Dual-Receive-Antenna
6. EOWEB - Earth Observation Data Service
7. EUMETSAT - European Organisation for the Exploitation of Meteorological Satellites
8. JAXA - Japan Aerospace Exploration Agency
9. JPL - Jet Propulsion Laboratory
10. InSAR - Interferometic Synthetic Aperture Radar
11. IRV - InSAR Radial Velocity
12. LOS - Line-Of-Sight
13. NOAA - National Oceanic and Atmospheric Administration
14. NSIDC - National Snow and Ice Data Center
15. OSI - Ocean and Sea Ice
16. SAF - Satellite Application Facilities
17. SAR - Synthetic aperture radar
18. SNR - Signal-to-noise ratio
19. SP-InSAR - Single-Pass Interferometic Synthetic Aperture Radar
20. TanDEM-X, TerraSAR - Environmental satellites
21. UAF - University of Alaska Fairbanks
22. VVC - Validation Velocity Component
23. XT - Cross Track

Glossary

This section demonstrates the most important terms and definitions of this work.

1. Across-track interferometry is a technique when two antennas are displaced one from another in the across-track direction and they both are flown along the same track [32].

2. Along-track interferometry - when two antennas are flown on separate tracks and displaced in along-track direction [32].

3. The baseline is a spacing between the two antennas [9].

4. Backscatter is the component of the outgoing radar signal which the target reverses straightforwardly backward the radar antenna [9].

5. Horizontal and vertical polarization. Horizontal is linear polarization with the line electric vector oriented in the horizontal direction in antenna coordinates and vertical polarization is obviously the same, but in a vertical direction [9].

6. Interferometry is a technique that uses the calculated differences in the phase, between two satellite passes, to detect slight changes on the Earth's surface (topography, motion) [32].

7. Interferometric Synthetic Aperture Radar (InSAR) - is a technique comprising phase measurements from subsequent satellite SAR images to observe some topographic or motion changes of the underlying surface with unprecedented scale, accuracy and reliability [9].

8. Interferogram is an image of the measured phase difference [32]. It is presented in radians of phase difference and is recorded as repeating fringes that each represent a full 2π cycle, because of the cyclic nature of phase.

9. Phase is a property of a periodic phenomenon. In radar remote sensing, the concept of phase is usually applied to the oscillation of electromagnetic waves [9]. The time delay between two waves is equivalent to the corresponding phase difference.

10. Radar coherence is one of the most important concepts for imaging radar systems such as SAR [3]. Coherence in the interferogram is a measure of

correlation between two signals, it ranges from 0 to 1 and can be used to examine the relation between two waves or datasets [9].

11. Radial velocity is the component of the velocity when an object is moving toward or away from the line-of-sight of an observer. It can be negative if an object is approaching (inbound) or positive if the object is moving away from the radar (outbound). This "radial velocity" component can be measured by Doppler radars [9].

12. Signal-to-noise ratio (SNR) is the comparative amount of additive noise. Signal noise is any undesirable or contaminating signal, which is competing with the desired signal [9].

13. Synthetic Aperture Radar is a coherent radar system that provides high-resolution remote sensing imagery [9].

14. X-Band is a frequency range from 12.5 to 8 GHz (specific wavelength 2.4 to 3.75 cm) within the microwave portion of the electromagnetic spectrum [9].

1 Introduction

Arctic sea ice cover has always been a crucial element of the climate system. It integrates the illimitable ocean, atmosphere and boundless land surface. It is notorious that nowadays mankind faces a problem called "Global Warming" – increasing in the average temperature of the climate system. One of the most important consequences of global warming is melting of sea ice in the polar regions. Therefore, polar regions, especially Arctic area, react strongly on the anthropogenic influence and temperature changes more than other parts of our planet. Significant changes of the sea ice cover that have occurred in the last decades, widely discussed all over the world and made the topic of global warming in the Arctic interesting for the scientific community. Sea ice variabilities in the Southern and especially Northern hemispheres, since the begining of the satellite observations, may not allow us to precisely answer on the question of global warming, due to lack of time series data. However, sea ice cover in the Arctic began to decline rapidly from the beginning of the new century. In September 2012, Arctic sea ice extent reached a record minimum since the start of satellite observations.

Sea ice is the main natural reason which is complicating shipping in the Arctic. The greatest threat to the ships, render the dangerous ice phenomena such as compression of ice, intense drift ice, narrowing of the navigable channel, adhesion of the hull, and others. Sea ice is a very dynamic structure. Sea ice floes drift due to several forces such as wind and ocean currents. Then ice breaks, fractures and openings occur, or if the ice pieces are pushed together they can form the deformation structures like ridges, rubble fields, hummock which can be very dangerous for shipping and offshore applications [14]. For safe navigation of ships, you need to pre-select the route and sailing time that is why we need to understand and calculate the drift of sea ice.

Currently, the most universal source of information to create ice charts are remote sensing data. In connection with obtaining such information, which is represented as a satellite image, necessity of creature new automated methods for processing this data is increasing. As a result of the work with satellite images, new algorithms for classification of ice formations and analysis of sea ice drift was created.

There are two types of calculation methods of sea ice drift: manual and automatic one. The first method of calculation of ice drift is manual, it is based on manual

identification and saving of the coordinates of identical ice features on a pair of synthetic aperture radar (SAR) images. The second type is automatic and it can be also classified by several types like cross-correlation, hybrid, keypoints tracking methods, etc.

For more than 30 years, spaceborne synthetic aperture radar systems have demonstrated their outstanding capabilities for numerous Earth observation applications that greatly benefit from the ability to acquire high-resolution radar images independent of sunlight illumination and weather conditions. With the introduction of interference methods in the early 1990s, the scope of applications has expanded significantly. [16]. In the first instance, radar interferometry was served in a purpose of topographic observations of Venus, Moon and Earth. Then it was adapted to measure motion of surface and was used to calculate the velocity of ocean currents [32]. InSAR combines the high spatial resolution of a conventional SAR on the order of meters with the possibility to measure radial target velocities, by using two SAR antennas. This antennas are detached by some remoteness in flight direction and get two pictures of the same scene with a time delay on the order of milliseconds [22].

Interferometry SAR method which was used in this work differs from the other automatic methods of the sea ice drift calculation, including polynomial, cross-correlation, hybrid, keypoints tracking methods, etc. The basic feature of InSAR is using the phase difference for the specific goals, such as calculation of the topographic variabilities of the underlying surface and the changes of the motion of the objects. For the calculation of the sea ice motion velocity and separation the sea ice on two particular zones, such as drift sea ice types and stationary sea ice types, interferometric phase difference was used, which is presented in the data as an interferogram. The interferogram was formed with image scenes from two SAR receivers. One of the main scientific goals of this work is to show the main advantages and gaps of the InSAR method in comparison with other methods of fast ice detection and sea ice drift calculation.

For applying of the InSAR method, 10 datasets from the TanDEM-X mission, for the test site area near Barrow, Alaska (Figure 1) were used. Every dataset consists of several files, including metadata, HH and VV polarization images, backscatter, coherence and phase images and the main for this study is interferometric phase difference (interferogram). The selected study period starts from early February and lasts until late May. It falls into the transition period between the summer and

winter hydrological navigation seasons in the Arctic, when the sea ice conditions of the Arctic seas are changing significantly.

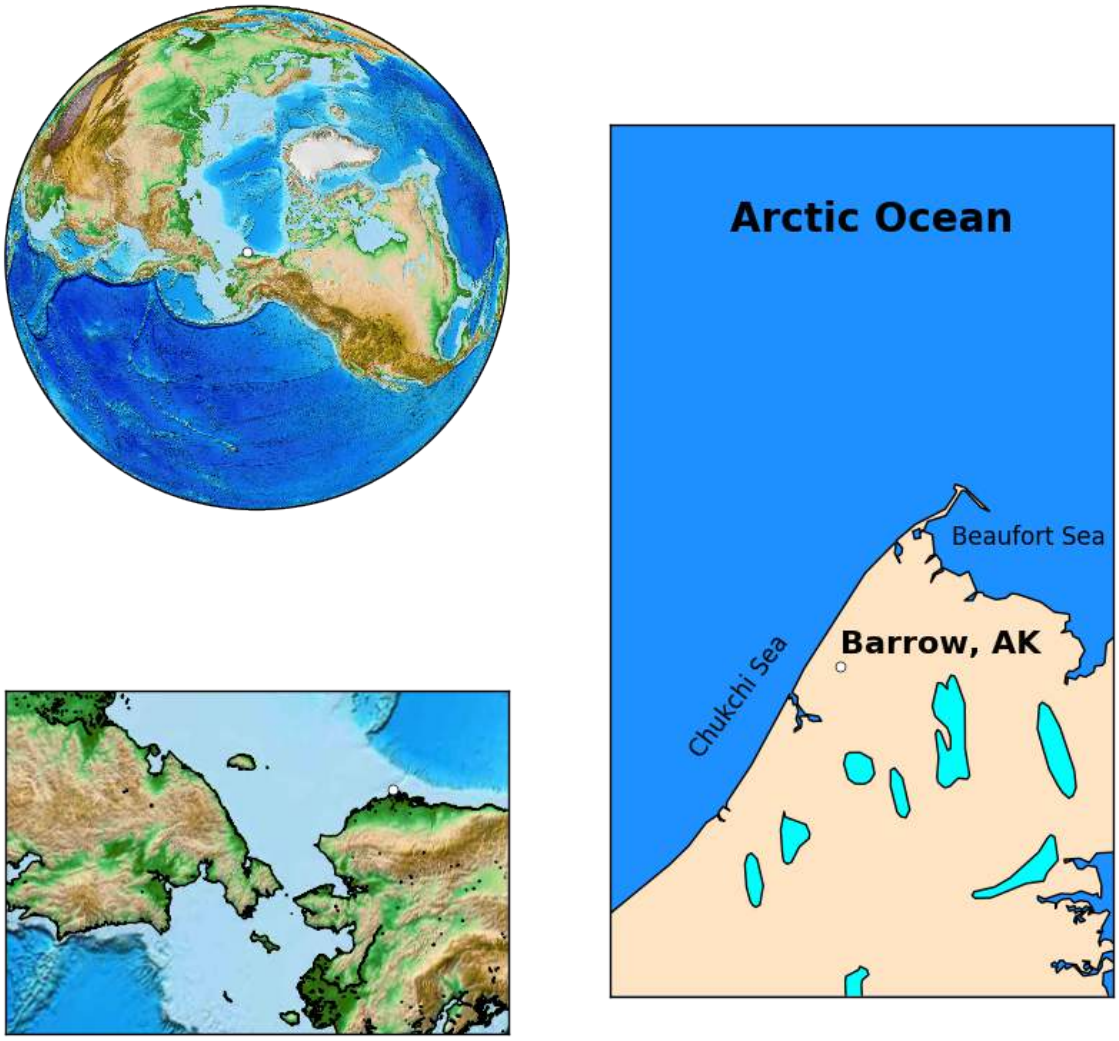

Figure 1: Maps of the selected test site area, near Barrow, Alaska.

2 Scientific questions

1. How is interferometric phase difference related to the line-of-sight velocity?
2. What is the advantage of InSAR method in comparison with other methods?
3. What are the new possibilities of the method, associated with the fast ice detection and calculation of sea ice motion?
4. What is the accuracy of the InSAR method?
5. What is the application of modern methods of analyzing remote sensing information in connection with climatic and oceanographic changes at the polar regions?

3 Selected test sites

One primary selected test site is the TanDEM-X supersite Pt. Barrow (Figure 2), which is the northernmost point of the United States of America. Point Barrow is a headland on the Arctic coast of Alaska, 14 km northeast of city Barrow. Barrow is also the largest native community in northern Alaska with more than 4600 residents. Point Barrow is an important region because it is marking the borders between two marginal seas of the Arctic Ocean, the Chukchi Sea and the Beaufort Sea. The elevation of Barrow is less than 20 m and the climate is depend strongly by the nearness of the ocean. The Chukchi and Beaufort seas cause a strong influence on air temperature and humidity in the ice free periods. In the early October, usually develops a stable ice cover with the approximate thickness of 10 cm and landfast within several weeks. The predominant land type in Barrow is tundra, which is formed above a potent permafrost layer [15].

This region was selected, because of several significant reasons. First and foremost, the sea ice conditions in the study area are well documented due to a long-term monitoring program conducted by the University of Alaska. The second and most important reason is that the sea ice motion can be derived from an onshore marine radar system in the range up to 11 km around Barrow, with the discreetness approximately every five minutes [14]. Consequently, this reasons allows to provide operational monitoring and analysis of sea ice conditions near Barrow, Alaska.

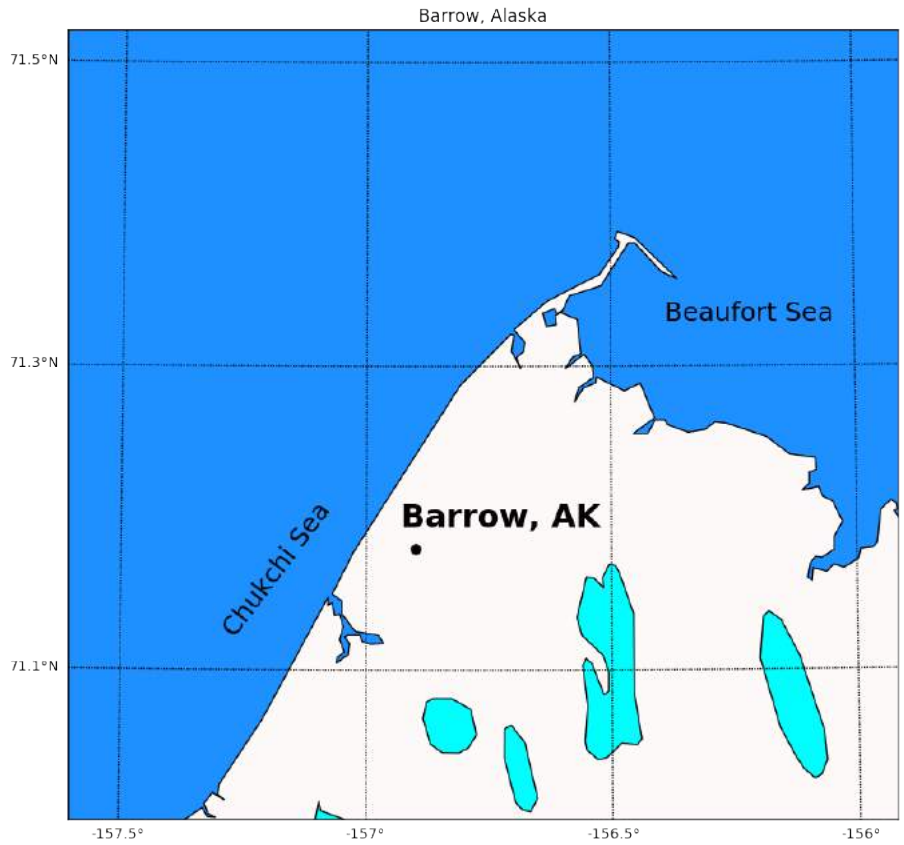

Figure 2: TanDEM supersite Pt. Barrow, Alaska. A marine X-band radar monitors the near-shore ice at ranges up to 11 km. Geo-referenced radar data are available in 5 minute intervals and can be used for motion vector retrieval.

4 Sea ice types

Sea ice is a component of a several disciplines, such as navigation, physics, climatology, meteorology, oceanography, marine biology, marine and offshore structural engineering. It is also an important part of the cryosphere and it continuously interacts with the ocean and the atmosphere. Sea ice plays a key role in the climate system, because it is one of the main indicators of global warming, therefore particular attention is paid to its variability [27]. The main part of sea ice drift velocities is found in the range from 0 to 30 km/day (10 km/day = 0.116 m/s) [14].

Sea ice cover of the northern hemisphere has changed significantly since the beginning of satellite observations. While in the Arctic there was a negative trend of ice changes in Antarctic, on the contrary, the area of sea ice grew. Figure 3 demonstrates the gradual decreasing of the sea ice extent in September and February for the Arctic region from the beginning of the satellite observations. The amplitude of seasonal fluctuations of the sea ice area in the Antarctic is greater than in the

Arctic region. Figure 4 demonstrates mean sea ice concentration in Arctic and for comparison in Antarctic in September and February. The observed negative trend in Arctic region may lead to opening a seaway connecting the Atlantic and the Pacific Oceans for marine navigation, this in turn will change the roles for naval transportation of goods and supplies during winter months in many northern countries [27].

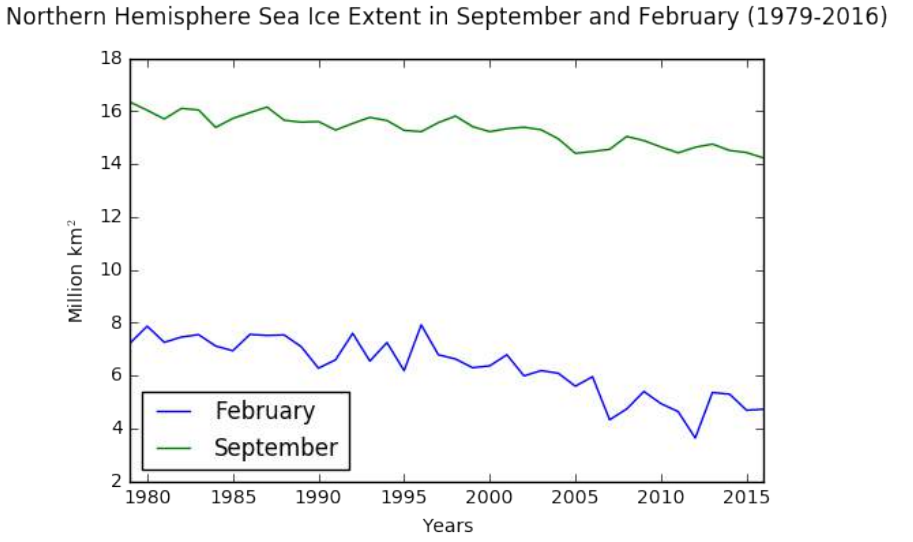

Figure 3: Northern Hemisphere sea ice extent in September and February from the beginning of the satellite observations. The data were obtained from NOAA. Sea ice extent provided by the National Snow and Ice Data Center (NSIDC) is available from 1979–2017 for the Northern Hemisphere.

For the creating of the ice maps and work with ice information, the nomenclature of sea ice was invented. It includes sea ice terminology, symbols for ice maps, descriptions of age characteristics of ice, etc. Nomenclature distinguishes many types of sea ice, but for this work not all of them are really important, because in the analysis of the sea ice conditions performed on the basis of the remote sensing data, not all the parameters of the sea ice cover, provided by the nomenclature, can be easily identified.

There are several goals of sea ice mapping, including retrieving different sea ice properties, such as the age and thickness of ice, position of the sea ice at a particular time and temporal changes of the sea ice cover. One of the main task of sea ice mapping is separating different sea ice categories one from another and, certainly, from the open water areas. With the advent of satellite observations of sea ice, there was a need to create new methods for processing satellite images,

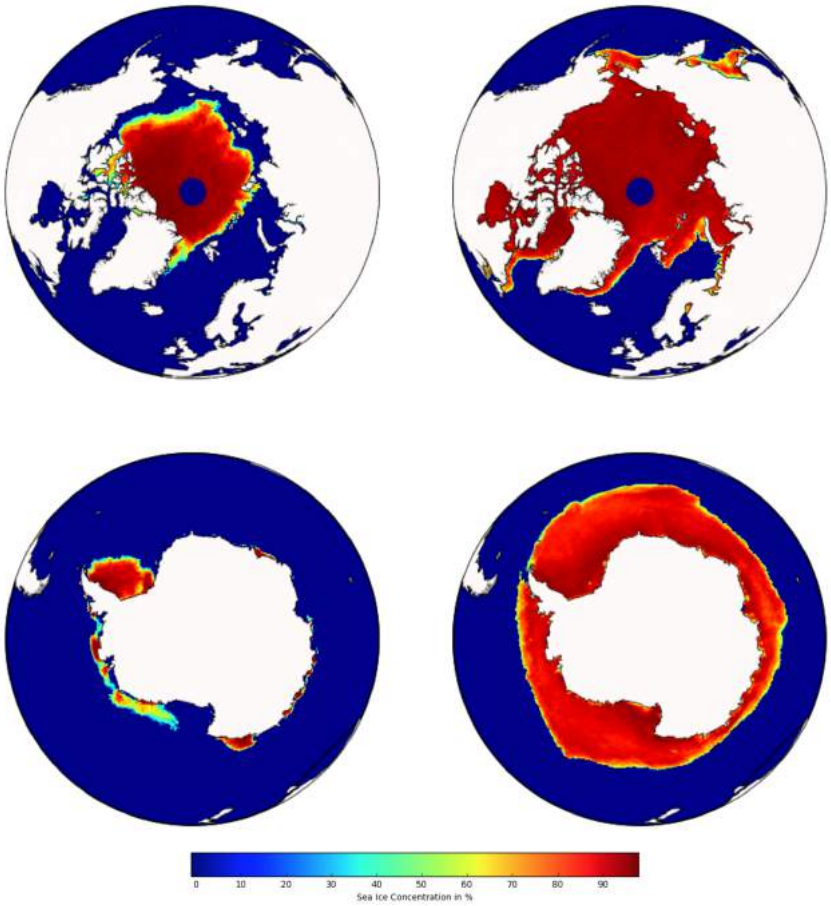

Figure 4: Maps of mean sea ice concentration in September and February in the Arctic (top) and Antarctic (bottom) obtained from the CERSAT/IFREMER dataset.

classification of sea ice and drift of ice. The appearance of sea ice in radar images is affected by several characteristics, including polarization, incidence angle, noise level, and spatial resolution of the respective SAR system or SAR imaging mode [5].

This section demonstrates a detailed description of the most important sea ice types, which are closely connected with the tasks of this work.

4.1 Fast ice

One of the main scientific goals of this work is to identify the fast ice zone and distinguish it from the drift ice. According to the nomenclature, there are several types of ice that are considered stationary, including fast ice, icefoot, grounded ice, stranded ice, grounded hummock, anchor ice [4]. The main stationary type of ice is fast ice, which will be discussed in this section.

Fast ice is consolidated solid ice that is attached to the shore, to an ice wall or to an ice front. It forms by freezing to the shore of the ice cover that is generating in

the coastal zone or as a result of freezing of drifting ice formations of any particular age category to the coast or fast ice. Fast ice can be preserved without fracturing for two or more years, transforming from first-year ice to multiyear ice or even to shelf ice. Vertical motion of the fast ice zone can be observed by dint of tidal oscillations. The fast ice width can vary in range from several hundreds of meters up to several hundreds of kilometers. Ice foot is a part of fast ice presenting a narrow fringe of ice directly attached to the coast with a shallow bottom and irresponsive to tidal oscillations that remain after the fast ice has moved away. Fast ice at the initial phase of formation which can consist of nilas and different types of young ice with a width up to 100-200 m is called young coastal ice. When mapping and coding the fast ice zone on the ice maps, the total concentration is not specified, because, according to the definition it is a priori equal to 10/10. [4].

Fast ice zone is significant due to several reasons. Fast ice is very important for the to coastal communities (indigenous nations of Arctic), because they use it for hunting, traveling and other features [19]. Sea ice is also important for oil and gas production, as the fast ice is formed in the coastal areas near the shipping routes. Furthermore, the stability of ice depends on the certain thickness level, so its conditions (occurrence, break-ups) can serve as an indicator of climatic state. In the last decades, several studies was employed, connecting with repeat-track interferometry over fast ice zones. For nearly stationary ice, deformations can be considered from small motions of parts of the ice cover relative to one another. These observations help to evaluate the rheology of sea ice [14].

Remote sensing observations are significant to studies, which are connected to the fast ice zone. The fast ice zone can be clearly identified on satellite images, because of motionless and contiguity to the coast. To determine the fast ice zone, a pair of images which is covering the same area with a certain interval is used, and the correlation between them is investigated. For the sea ice observations various types of remote sensing can be used, but the main is active microwave technique, based on Synthetic Aperture Radar data processing, which has a high spatial resolution and does not depend on weather conditions. Based on the determined tasks, several methods can be used to validate the accuracy and correctness of the results [13].

4.2 Drift ice

Drift ice is any ice at the sea surface, except fast ice, icefoot, grounded ice, stranded ice, grounded hummock, anchor ice, that have a possibility of movement under the action of the several reasons, such as wind, currents and tides. Eventually, the total and partial concentrations of drifting ice constantly change, because of the dynamic processes (drift, divergence, convergence). If drifting ice is knocked together into a large unified mass, it is called pack ice. According to the nomenclature, there are several types of floating ice, which are divided according to their size, including pancake ice, ice cake, ice breccia, brash ice and giant, vast, big, medium, small ice floes [4].

Drift ice is very important due to several reasons. One of the main reason is navigation and prevent of some hazardous situations which are connected with dangerous ice phenomena and can occur on the main routes of Arctic region, including Northern Sea Route, Northeast and Northwest passages.

Remote sensing observations are also important in drift ice studies. To determine the zones of drifting ice and track the direction and speed of their motion, a pair of images with a particular interval between them is used. By the dint of a pair of images it is possible to trace in which direction the ice moves in a certain area and calculate the velocity of its moving. There are several methods of automatic sea ice drift calculation, including polynomial, cross-correlation, hybrid, keypoints tracking and others.

5 Datasets description

For creating the radial velocity maps for the fast ice detection and sea ice motion calculation and validation of the InSAR method, several types of data were used. Table 1 demonstrates the instruments and data formats which were used in this study. The main data were obtained from TanDEM-X mission, which provide 10 datasets with satellite images, including coherence, backscatter, phase, HH and VV polarization images, metadata files and also interferograms which have been produced over the study area and were readily provided in the product. For the comparison and validation of the InSAR method, coastal radar images and vector tracking were used.

Table 1: List of using datasets.

Instrument	**Data**	
	Composition	**Format**
TanDEM-X, TerraSAR-X	coherence, backscatter, interferogram and metadata files	xml, tif, flt
CERSAT/IFREMER	sea ice concentration	NetCDF
GCOM-W1 (AMSR2)	sea ice concentration	NetCDF
Coastal Radar (Furuno 10 kW)	radar images, vectors tracking	png, txt

5.1 Coastal radar images

Sea ice that is close to the shore is monitored used Furuno 10 kW, X-band marine radars. They located close to the shore on rooftops and the distance of their operating is in the range of 11 km. UAF provides remote operations using Xenex digital controllers. There are two main types of marine radar frequencies, known as "X" and "S" band. "X" band provides higher resolution images because of its higher frequency, 10 GHz, while "S" band is less affected by rain and fog and have a lower frequency, 3 GHz. For the obtaining important information about movement, deformation, stability of the coastal sea ice cover, radar backscatter images are produced [31].

The radar is located in Barrow downtown atop the 4-story building and it works the whole year. UAF has operated this coastal sea ice radar intermitting since the 1970s. The data is available in near real time from http://seaice.alaska.edu/gi/observatories. Figure 5a demonstrates the example of the coastal radar image and Figure 5b shows the same image with the area marking the continent and with parallels and meridians of the selected test site area.

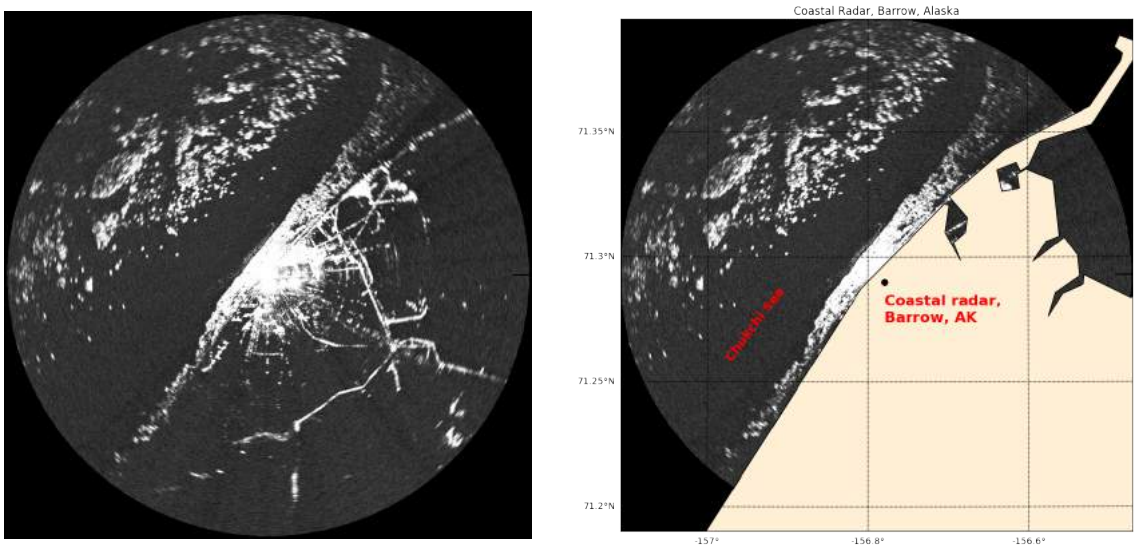

(a) Radar image example

(b) Coastline, parallels and meridians

Figure 5: Example of the coastal radar image and location of the coastal radar with coastline, parallels and meridians of the selected test site near Barrow, Alaska. Images are obtaining approximately every 5 minutes and provided by the University of Alaska. The dimension of the image is 20 x 20 km with 20 m resolution.

Dark regions of this image may indicate the open water areas, however, sometimes they might also display smooth ice or shadow zones behind large features. White color, on the contrary, indicates older sea ice types (young ice, first-year ice, second-year ice, multi-year ice) and the coastal zone near to selected test site. Some atmospheric features, such as fog or rain, can rarely be seen in the radar imagery as well [31].

The data from coastal radar are collected in range-azimuth space with 512 samples per range line and up to 4096 lines per rotation. The coastal radar system records imagery approximately every 4-5 minutes. The time interval between the images may vary due to small changes in rotation speed of the radar antenna [18].

5.2 Coastal radar vectors

This section demonstrates the data which will be used in the following sections for the validation of the InSAR method for the sea ice theory. The vectors, on the (Figure 6), shows the motion direction of the concrete ice formation in the selected test site area, near Barrow, Alaska. The vectors were created for several examples, which correspond with satellite data in time, and stored in the form of txt files

with vector tracking information, which consist of the longitude, latitude and u, v components of the vectors. The motion of particular ice formations was obtained by dint of manual drift calculation of 5 images with interval between each pair of images equal to 5 minutes.

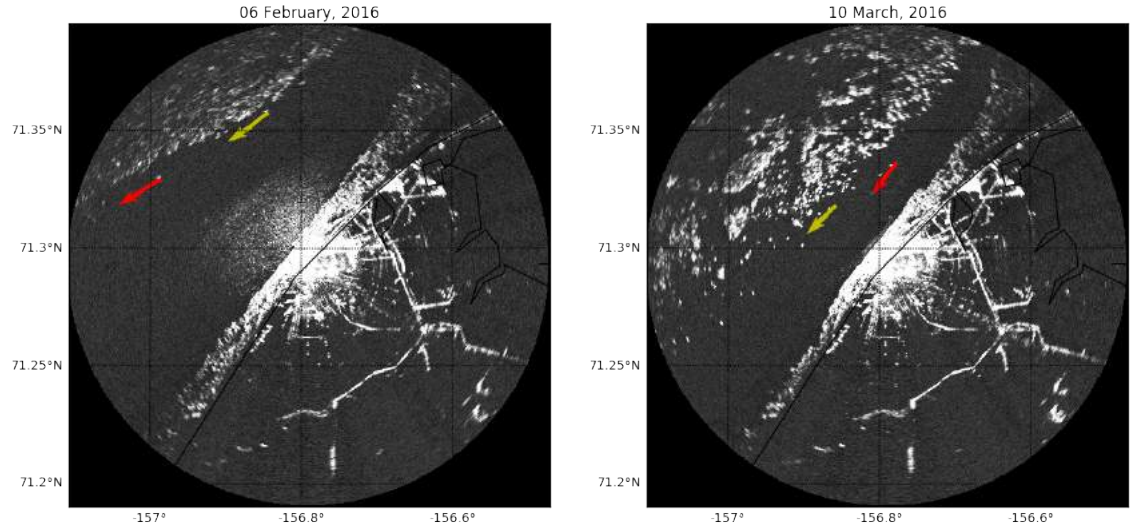

Figure 6: Example of the coastal radar images with several vectors tracking for the particular ice formations, near Barrow, Alaska.

5.3 Satellite data from TanDEM-X mission

The main satellite data which were used in this study was obtained from TanDEM-X satellite mission(Figure 7). TanDEM-X mission consist of two German Earth-observation satellites TerraSAR-X and TanDEM-X. The first of these two satellites, TerraSAR-X, has been working since 2007. TerraSAR-X was primary payload as an X-band radar sensor with a large range of different modes of operation, that makes it possible to record images with different swath widths, resolutions and polarizations. Thus, TerraSAR-X offers space-based observation capabilities, that were unavailable before [7]. After three years of operating, it has been lined up with its twin satellite, TanDEM-X. Flying in close formation, merely a few hundred metres distant, the two satellites are picturing the territory underneath them synchronously, from different angles. These images are converted to precise elevation maps with a high resolution. The TanDEM-X satellite follows the TerraSAR-X design with minor modifications such as an additional S-band receiver which derives status and position information sent from TerraSAR-X and etc [7]. TanDEM-X (TerraSAR-X add-on for Digital Elevation Measurement) is the first

single-pass radar interferometer in space that employs two SAR satellites flying in a closely controlled formation [16]. The DEM is a digital model or 3D representation of the surface relief. The main goal of the TanDEM-X mission is to produce high-resolution and wide-area radar images which are congeneric in quality, unequalled in accuracy and are independent of the weather conditions. These satellites have a unique geometric accuracy that is unparalleled by any other spaceborne sensor. Table 2 demonstrates some general characteristics of TerraSAR-X and TanDEM-X satellites. According to this table the satellites have similar characteristics.

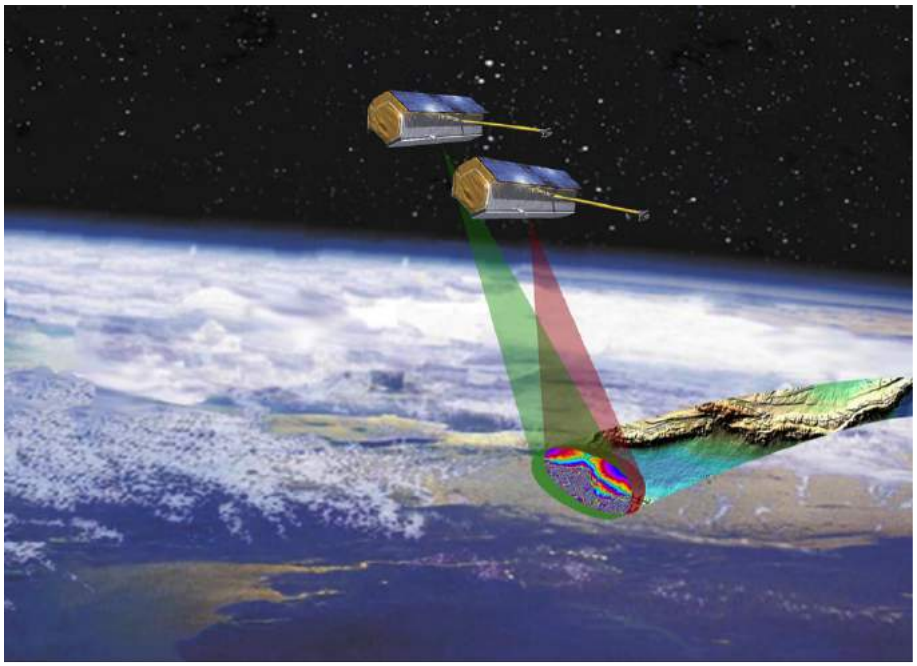

Figure 7: Satellite mission TanDEM-X, source: http://www.dlr.de/.

Table 3 illustrates the types of satellite frequency bands. The choice of frequency for transmitting data from the earth station to the satellite and from the satellite to the earth station is not arbitrary. Frequency of the signal, for example, depends on the absorption of radio waves in the atmosphere, as well as the necessary dimensions of the transmitting and receiving antennas. The frequencies at which the transmission from the earth station to the satellite occurs are different from the frequencies used for transmission from the satellite to the earth station [9].

Table 2: Characteristics of the TerraSAR-X and TanDEM-X satellites.

Characteristics	**Satellite**	
	TanDEM-X	**TerraSAR-X**
Launch	21 June 2010	15 June 2007
Launch site	Baikonur, Kazakhstan	Baikonur, Kazakhstan
Orbit altitude	514 kilometers	514 kilometers
Orbit inclination	97.4 degrees	97.4 degrees
Radar frequency	9.65 gigahertz	9.65 gigahertz
Period of Operation	2010 - present	2007 - present
Agency	DLR	DLR
Resolution	1-16 m	0.24-260 m
Orbit Repeat Cycle	11 days	11 days
Band/Frequency (GHz)	X-band/9.65	X-band/9.65
Wavelength (cm)	3.11	3.11

Table 3: Satellite frequency bands.

Frequency band	**Frequency range (GHz)**	**Wavelength range (cm)**
L band	1-2	15-30
S band	2-4	7.5-15
C band	4-8	3.75-7.5
X band	8-12	2.5-3.75
Ku band	12-18	1.67-2.5
K band	18-27	1.11-1.67
Ka band	27-40	0.75-1.11

In this work 10 datasets of the satellite images from the TanDEM-X mission were used. The satellite data consist of interferometric phase difference in form of interferogram, coherence, backscatter images and etc. There are several parameters that are not fixed and has changing depending on the orbit, including along-track baseline, effective baseline, incidence angle, corner coordinates of the image. There are also few parameters that are fixed for 10 datasets, for example, all the TanDEM-X data has HH and VV polarization channels, R look direction, bistatic cooperative mode. Figure 8 demonstrates the examples of raw satellite images, including HH

polarization(Figure 8a) and coherence(Figure 8b). According to the images, it is difficult to identify the fast ice or drift ice zone, that is why subsequent processing with interferometric phase difference is needed.

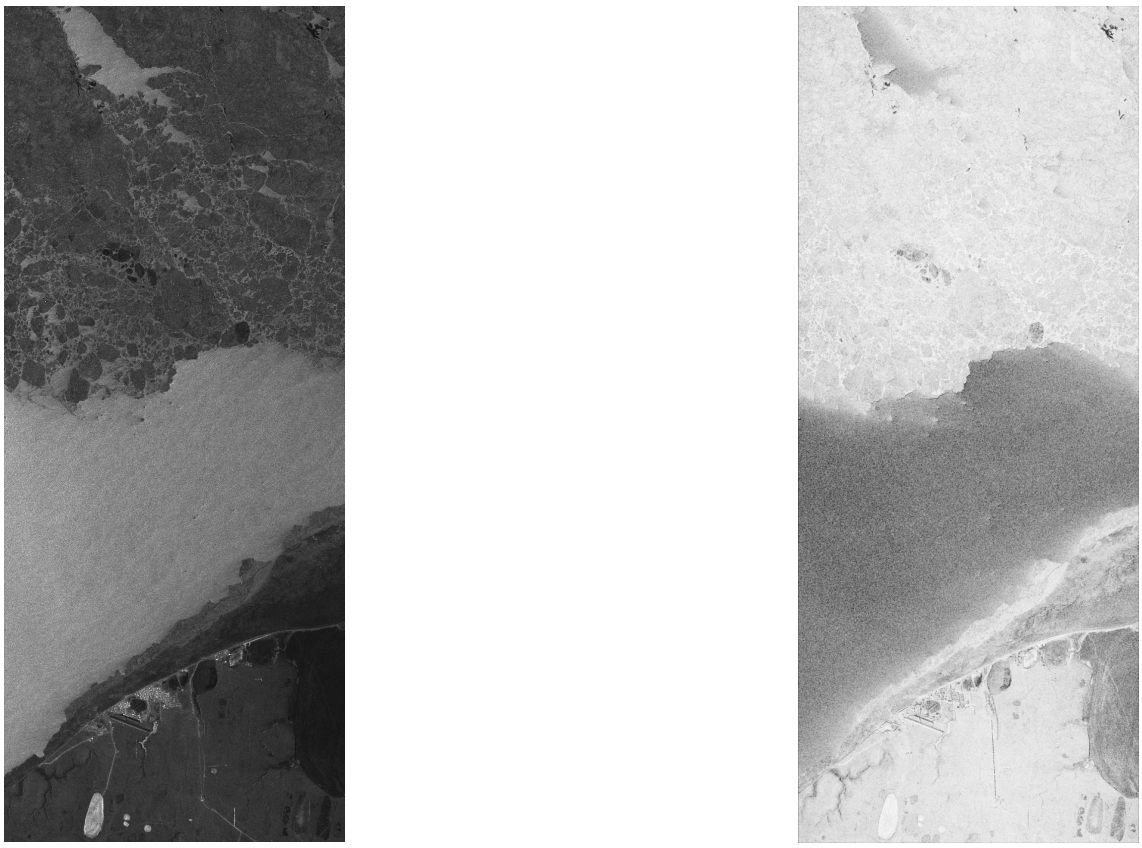

(a) HH polarization (b) Coherence

Figure 8: Examples of the satellite images, including HH polarization and coherence images.

6 Potential Applications and Products

Interferometric phase observations contains several potential applications and products, such as topography of the underlying surface and motion of the objects, in our case this is the velocity and direction of ice drift. According to the scientific questions, goals and purposes of this work, the "motion" application is much more important, for instance for the fast ice detection, calculation of the velocity/direction of sea ice and ocean currents motion.

6.1 Topography

The surface topography of ice needs to be noted for the evaluating the transfer of momentum among the atmospheric and the ice boundary layers. Designation of ice freeboard at the margins in the fields between ice and water areas (leads, polynyas, melt ponds) plated with thin ice is essential for the thickness of the ice extracts [14].

Due to the altitude change on sea ice are in the range of only a few meters, the exactness of height estimation must be not less than 0.5 m. In order to judge about the potential of single-pass InSAR for retrieving the sea ice surface topography was analyze the height of ambiguity(Equation 1), the phase noise(Equation 2), and the height error(Equation 3):

$$h_a = \frac{\lambda H \tan\theta}{pB_n} \tag{1}$$

$$\sigma_\phi = \sqrt{\frac{1}{SNR}} \tag{2}$$

$$\sigma_h = H \tan\theta \frac{\lambda}{2\pi p B_n} \sigma_\phi \tag{3}$$

Here we have λ – wavelength, H – orbit height, θ – incidence angle, B_n – baseline perpendicular to the line-of- sight (LOS), SNR – signal-to-noise ratio, and p = 1 if one image is acquired in mono-static and the second in bi-static mode, and p = 2 if both images are acquired in mono-static mode.

6.2 Sea ice motion

Sea ice is a dynamic medium and it moves on a temporal scales of hours, approximately 10-30 km/day (30 km/day = 0.35 m/s) and can reach up to 90 km/day. Exploration of the sea ice motion is so appealing due to several reasons. One of the reasons is sea ice navigation and prevention of dangerous situations which are connected with the dangerous ice phenomena, that can occur on the routes which are close to the poles. Therefore, observations of the sea ice drift is important for the safe route navigation. Also significant reason is the ice motion on the scale of several hundred kilometers, which are driven by the large-scale atmospheric circulations and influence the regional balance of sea ice masses in the polar regions [14]. Sea ice drift also affects on many parameters such as sea water salinity and temperature. Salinity and temperature of the sea water, in turn, produce an effect on the

interaction and heat transfer between the ocean and the atmosphere.

The focus on sea ice drift consists of two elements: (1) the motion of the sea ice between the data acquisitions of image 1 and image 2 may lead to decorrelation effects which have an impact on the retrieval of ice surface topography, (2) single-pass interferometry gives an alternative means of evaluating the momentary LOS ice velocities, moreover using the Doppler-frequency approach [14]. The phase shift ϕ is proportional to the change in distance of the resolution element that occurs in the time it takes for the rear antenna to move to a place of symmetry with respect to the front antenna [11]. The interferometric phase ϕ (Equation 4)for a baseline B_{al} in along- track direction and the corresponding velocity error σ_u (Equation 5) are:

$$\phi_{al} = \frac{2\pi puB_{al}}{v\lambda} \tag{4}$$

$$\sigma_u = \frac{v\lambda}{2\pi puB_{al}}\sigma\phi \tag{5}$$

with v – ground velocity (approximately 7 km/s for TanDEM-X), u – radial (LOS) target velocity, λ – radar wavelength, B_{al} – along-track (AT) baseline, and p - see above.

It should be clarified that only the LOS component of the sea ice drift velocity is measured and it is a snapshot of the instantaneous velocity field so it has limited use for scientific purposes and operational sea ice monitoring [14].

7 Methods

Sea ice observations performed from the vessels and coastal stations has a history of more than a hundred years. However, regular sea ice charting has evolved only with the advent of aircrafts and satellites. Until 1980, the main method of observing sea ice was aircraft survey, but later its place was taken by satellite remote sensing which became now the most important observation method.

The first satellite sensors used visible and infrared channels for the sea ice exploration. By the late 1960s, it became obvious to everyone, that visible sensors are not capable of providing full-scale observations due to the inability to work in the in bad weather conditions. Sea ice exists in regions that are dark for several months

and are frequently cloudy. The visible sensors were replaced by microwave remote sensors, which are now the main ones providing sea ice observation data [26].

Microwave remote sensing, using microwave radiation with specific wavelengths from about one centimeter to a few tens of centimeters and enable observation in all weather conditions without any weather restrictions like cloud or rain. There are two general classes of microwave remote sensing techniques: passive and active. Passive involves radiometers and active – radars. Whereas, active microwave sensors divided into five classes: synthetic-aperture radar, side-looking airborne radar, scatterometers, altimeters, meteorological radars. As suggested by the name, SAR employs synthetic-aperture antenna-processing techniques, by comparison the other sensor systems typically use real-aperture antennas [32].

A synthetic aperture radar is an imaging radar, and it is fixed on a moving platform. Electromagnetic waves are relayed sequentially, likewise a conventional radar, and the backscattered refraction is collected by the radar antenna [20]. SAR is a coherent active microwave imaging method that generates high-resolution remote sensing imagery. In remote sensing, SAR is used for mapping the scattering properties of the Earth's surface in the corresponding wavelength interval. Many physical and geometric characteristics of the imaged scene contribute to the grey value of a SAR image pixel. Scene inversion afflict with this high ambiguity and needs SAR data taken with diverse characteristics of wavelength, polarization, time, incidence angle, etc [2].

Satellite and airborne SAR systems are used for a large range of tasks that are connected with retrieval of information about the conditions of the sea ice cover [5]. Appropriate instances of this tasks are drift and deformation of ice, ice type classification, characterization of the ice growth and surface topography, determination of melt pond coverage on the ice, observations of the marginal ice zones and polynyas, fast ice detection and etc. To measure the sea ice drift is better to use SAR data, which do not reliant on the light and clouds as it is essential to the polar regions.

7.1 Interferometry SAR

7.1.1 Brief history of radar interferometry observations

In the first instance, radar interferometry was served in a purpose of land-based observations of Venus. It was helping to divide equivocal range-Dopper echoes re-

verberated synchronously from Venus's northern and southern hemispheres. Afterwards, the technology was used to receive altitude information about the surface of the Moon and Venus. In addition, radar interferometric methods were used to measure the Earth's surface topography from satellite platforms and aircraft as well. In 1974, Graham reported about observations of interference fringes modified by Earth surface topography, they were recorded by an aircraft interferometric radar [32].

Zebker and Goldstein, at the beginning of the 1980s, put in force an airborne interferometric radar system on a NASA CV990 aircraft which was outfitted with a digital data recording system. It was possible to record two radar channels, one from each of two separately-located radar antennas, and later elaborate the data using JPL digital correlator system. They showed that the phase deviation between the two signals included enough information to reconstruct the topography of the imaged radar scenes. Besides that, the idea to make adjustments to the measured data for event-present deviations of the aircraft flight path translated into reality, it was possible to cause artifacts in the radar images. Consequently, the digitally correlated radar interferometric technique can supply digital elevation information with an exactness on the order of a few meters [32].

Furthermore, Zebker and Goldstein are known for extending the capacities of radar interferometry by analyzing the capability of forming interferograms using radar antennas transposed along the direction of flight, respective to temporal rather than spatial separation of the images. In consequence of this technique, nowadays we are able to measure currents, the movement of the surface, velocity of ocean waves with good accuracies [32].

7.1.2 InSAR Principles

InSAR method is one of the fastest growing parts in the field of remote sensing and Earth sciences. Interferometry SAR is a powerful and well-established remote sensing technique used to measure several parameters such as topography and the motion of the surface [16]. There are several types of interferometric survey techniques: along track which can be along-track with two independent radars separated in time and across-track that can be subdivided into cross-track with two independent radars each with its own transmit/receive antenna, cross-track with common transmit antenna, but separate receive antennas (Figure 9). The two antennas can

be separated one from another in the XT direction. It means that two antennas comprising the interferometer are flown on parallel, separate tracks and it is called cross-track interferometer [33]. Alternatively, the two antennas can be flown along the same track, with one displaced from the other by a certain distance, which is called baseline, or flown at a different time, and we refer to this geometry as an AT interferometer. Cross-track and along-track baselines ranging from 150 m to 10 km and from 0 to several 100 km, can be precisely set depending on the particular requirement of the measurements [28]. The main idea of the along-track interferometry, which is used in this work, is the repeated observations of a scene with nearly identical geometry and with a given temporal lag. If an target is moving and the motion of this object has a non-zero component in the LOS direction, the resulting change of the slant-range will result in an interferometric phase [17]. InSAR techniques also subdivided into single and multi-pass or repeat-pass interferometry. In single-pass interferometry, the two antennas are mounted on a single platform and the data are collected synchronously. In multi-pass interferometry, data collections are made at different times using either multiple platforms or multiple passes over the data collection area with the same platform. For very slow motion, such as those connected to terrain subsidence, these temporal scales are in the range of days to months, or even years. For such purposes is appropriate to use repeat-pass interferometry. For large velocities, including ocean currents, sea ice drift, these scales are typically in the order of milliseconds to tenths of seconds. This is the area of a single-pass along-track interferometry [17]. By exploiting the phase difference between pairs of coherent radar signals, SAR interferometry allows relative range of calculations with subwavelength accuracy [32].

InSAR combines the high spatial resolution of a conventional SAR on the order of meters with the possibility to measure radial or line-of-sight target velocities, by using two SAR antennas which are detached by some remoteness in flight direction and get two pictures of the same scene with a time delay on the order of milliseconds [22]. InSAR uses the phase inequalities of no less than two complex-valued SAR images that were obtained from different orbit collocations and/or at different times. The information from the interferometric sequence of data can be exploited to several geophysical quantities, as for instance, topography, distortion (volcanoes, earthquakes, ice fields), glacier flows, ocean currents, vegetation properties, etc [2].

A radar echo contains amplitude and phase information. The majority of imag-

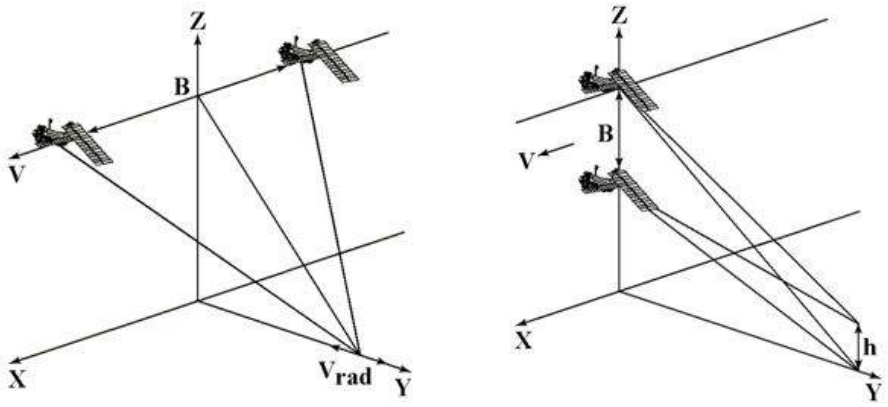

Figure 9: Geometry of the survey for along-track and across-track interferometry, source: http://www.racurs.ru/wiki/index.php

ing radar applications use algorithms that utilize only the amplitude to extract geophysical and biophysical information about the imaged scene and in some cases also used the phase difference between the HH and VV polarized scattering amplitudes. Such calculations of a phase difference is known as interferometry, which is a well-developed technique in optics [32]. Radar interferometry allows us to calculate the surface elevation of individual image pixels. It leads to the generation of topographic maps with height information. Radar interferometry is also used to measure surface motion, for example ocean currents or sea ice drift velocity/direction retrieval [25]. Applications of InSAR techniques for the motion and deformation of pack ice can be retrieved only in a single-pass mode because of temporal decorrelation. This condition is not so important for fast ice, because it can be "fastened" to the coast and remains stationary for days to weeks [14].

7.1.3 Interferometric Phase Difference

The interferometric processing and retrieval of surface height and motion is based on the phase distinctions between two radar signals from the same surface area, but from different sensor positions [1]. In this work, we are more interested in the surface motion calculation. By altering the imaging geometry to an along-track interferometry, it is possible to use the InSAR to measure surface motion, rather than elevation. The geometric interval between two radar locations is called baseline and consists of two main components: along-track and across-track component. The tracks are differ one from another, the along-track is oriented in parallel and the across-track is perpendicular direction to the satellite velocity vector. The along-track baseline

is the reason of time lag between two signals received from the particular surface area. This lag can change from several days in repeat-pass, to a few microseconds in single-pass InSAR. The result is the image that shows spatial distribution of the interferometric phase differences and it is called interferogram. The phase difference can be in range from 0 to 2π. One of the most important concepts is that interferometric phase difference is directly proportional to the radial velocity component of the object [11]. In the interval of time, between observations, the object is moving towards or away from the radar, and thus the phase of the radar signal changes [32]. But if the object is not moving, then the phase is remains unchanged, and after the calculation of the radial velocity this object can be easily identified by homogeneous field of zero velocity, what works great in case of fast ice detection. Another important concept is coherence, which in the interferometric studies means the correlation between two signals. In the unfortunate case the interferogram may contain only noise-like patches which indicates total decorrelation between the received signals. The contiguous patterns of recurring color cycles indicates continuously increasing or decreasing phase differences between well-correlated signals [6]. The interferometric phase difference $\Delta\phi$ is determined by this equation:

$$\Delta\phi = \Delta\phi_{topo}(B_{ac}) + \Delta\phi_{mov}(B_{al}) + \Delta\phi_{noise} + 2\pi n \tag{6}$$

According to Equation 6, the calculated interferometric phase difference may contain several types of information: change of surface height of the image $\Delta\phi_{topo}$, surface motion measured between the reception of signals $\Delta\phi_{mov}$ and noise $\Delta\phi_{noise}$ [6]. The noise is extremely important part of the processing of satellite images and can be a reason of some errors in the interferogram. There are three main sources of noise in the phase measurements of an interferogram, including the receiver thermal noise, "speckle" effect and antenna effect [12]. First is thermal noise, caused by some dark areas in a scene which in turn have low reflectivity, hence low signal-to-noise ratio. Second is "speckle" effect, which means that each resolution ellement in a radar image contains of a collection of small scatterers and they reflects their individual amplitude and phase. Consequently, significant part of the image will have low signal-to-noise ratio. Third is an antenna effect, which is explained by the fact that two antennas are not in the same place and any resolution element displayed slightly different in each image [12].

7.1.4 Radial velocity calculation

The ice motion case was studied using standard TanDEM CoSSC data products, obtained from EOWEB archive. The interferometric phase difference is readily provided in the product as an interferogram. Table 4 demonstrates the date of reception and main parameters of the satellite images, including along-track baseline, effective baseline, incidence angle and height of ambiguity. The along-track baseline values are used for the calculation of the radial velocity by dint of interferometric phase difference.

Table 4: Processing parameters for the data

Acquisition date	**Baseline, m**		**Incidence Angle**	**Height of ambiguity, m**
	Effective	**Along-Track**		
2016-02-06	129.176	-174.087	20.877	-23.798
2016-02-17	132.387	-90.941	20.877	-23.230
2016-02-28	137.061	-97.616	20.867	-22.427
2016-03-10	141.421	-81.967	20.870	-21.739
2016-03-21	146.297	-95.240	20.871	-21.016
2016-04-01	151.029	-97.729	20.875	-20.362
2016-04-12	155.292	93.907	20.835	19.765
2016-04-23	160.322	105.106	20.839	19.148
2016-05-04	165.056	104.220	20.829	18.590
2016-05-26	173.970	104.339	20.831	17.640

The single-pass ATI system is well suited for the phenomena, which velocities are in range of 1 m/s, such as ocean currents, sea ice motion, etc. [17]. The radial velocity can involve negative and positive values depending on the direction of motion (towards or away from the radar movement). Nevertheless, if an object is not moving at all or moving sideways, so that its distance, related to the radar, does not change, the radar will record zero radial velocity for this object [6].

The Equation 8, which was obtained after the transformation of Equation 7 [30], was used for the calculation of the radial velocity component from the interferometric phase difference.

$$\Delta\phi = \frac{4\pi}{\lambda}\frac{B_{eff}}{V_s}V_{los} \tag{7}$$

$$V_{los} = \frac{\Delta\phi}{4\pi}\frac{\lambda U_s}{B_{al}} \tag{8}$$

with $\Delta\phi$ -interferometric phase difference from $-\pi$ to π, B_{eff} - effective baseline, B_{al} - along-track baseline, λ - the radar wavelength, U_s - the sensor velocity. The $\Delta\phi$ values are presented in the form of interferogram (matrix of the interferometric phase difference). For TerraSAR-X, the sensor velocity value U_s is approximately equal to 7,600 m/s and radar wavelength λ for X-band systems is respectively equal to 0.0312 m. After the transformation of the Equation 7, it was decided to use B_{al} instead of B_{eff}. Along-track baseline B_{al} is not fixed and changes depending on the orbit as can be seen from the Table 4.

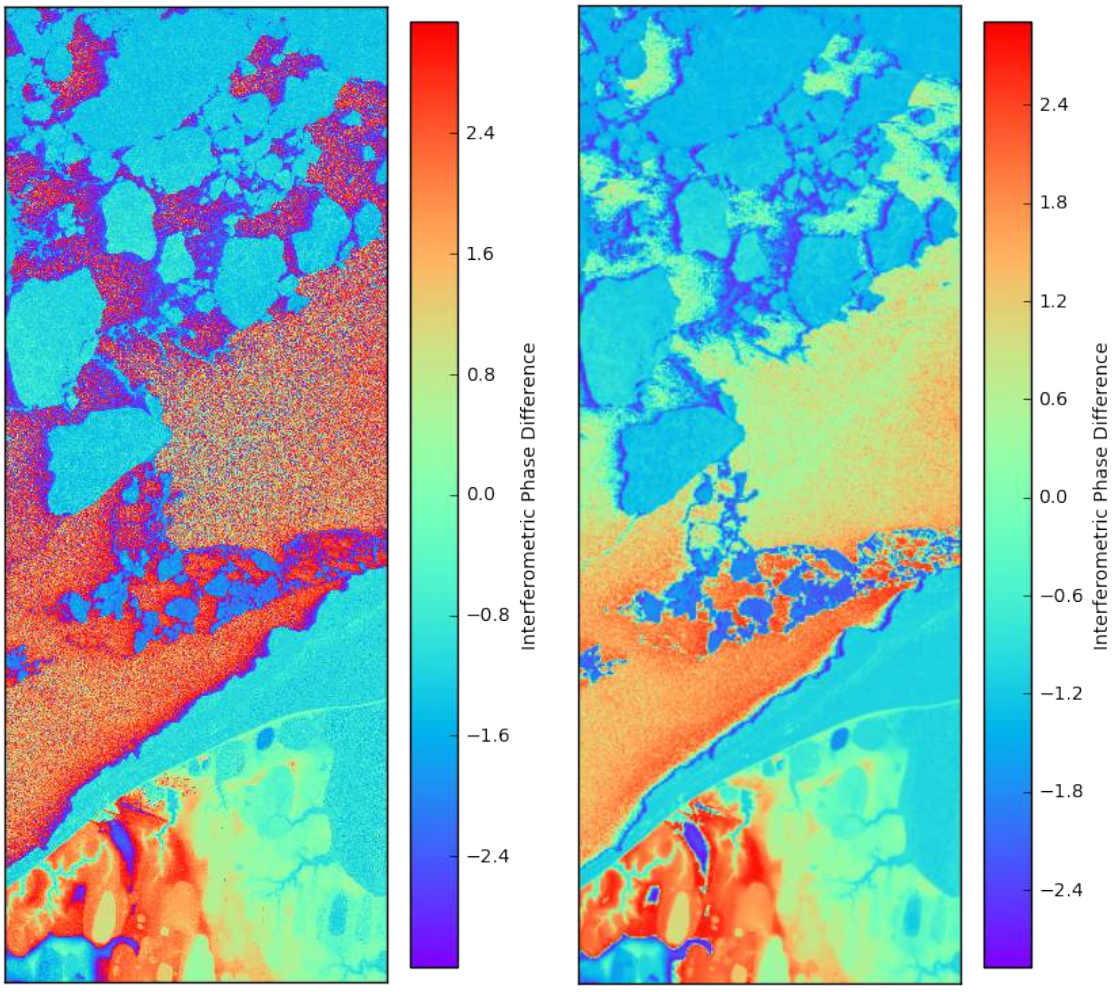

Figure 10: Example of raster generalization. The original interferogram (left) and interferometric phase difference after generalization.

In addition, to simplify the work with the interferometric phase difference and obtain better results, it was decided to use raster generalization. Raster generalization was introduced mainly for fast ice detection purposes (the separation of homogeneous fields of stationary ice). Generalization is the process, which removes small isolated regions from a classified image. Regions, which size is larger than a certain number of pixels, will remain on the image. Figure 10 demonstrates the example of a generalized output. The first figure is the original interferogram and the second one is the interferometric phase difference image after generalization. According to the Figure 10, small regions have disappeared from the generalized image (left), which, in turn, allows to easily identify the fast ice zones.

8 Results

This section demonstrates the results of the accomplished work with detailed description of all the constructed images. Table 5 illustrates the availability of the satellite images from the TanDEM-X mission, coastal radar images and vectors tracking data, which were used for the validation, with the date of their reception. The blue colored cells indicate the dates with visible fast ice zone, which will be important for the phase offset calculation.

Table 5: List of acquired TanDEM-X and coastal radar images.

Acquisition date	**Images**		**Vectors**
	TanDEM-X	**Coastal radar**	**Tracking**
February 06, 2016	+	+	+
February 17, 2016	+	+	+
February 28, 2016	+	+	+
March 10, 2016	+	+	+
March 21, 2016	+	+	+
April 01, 2016	+	+	
April 12, 2016	+	+	+
April 23, 2016	+	+	+
May 04, 2016	+	+	
May 26, 2016	+	+	

8.1 Sea ice conditions nearby Barrow, Alaska

The sea ice concentration data were obtained by dint of AMSR2 radar, which is located on board of JAXA on the platform GCOM-W1 and received in NetCDF format from the EUMETSAT OSI SAF source [10].

According to the nomenclature, the concentration of sea ice is a term that describes the relative amount of area covered by ice, compared to some test area. It is measured in percentages. A value of 0 means that there is an ice-free area, while a value of 100 means that the region is completely covered by ice [4].

For the direct analysis of the satellite images from TanDEM-X mission, first of all, it is necessary to analyze the sea ice conditions in the selected test site area, for the chosen study period. The selected test period occurs at the time of the transition between the summer and winter hydrological navigation season in the Arctic. This is the time when the sea ice conditions in the Arctic seas are changing rapidly and the shipping routes become ice-free. The summer hydrological season usually begins in May and lasts until September. Figure 11 demonstrates the isolines of sea ice concentration for several examples, around selected test site Barrow, Alaska. Blue color indicates the open ocean areas, leads, polynyas where sea ice concentration is less than 10%. Besides that, white color shows the sea ice concentration in the interval of 90-100%. As it is evident from the images, in general sea ice concentration lightly decreasing from the beginning of February (Figure 11a) till the end of May(Figure 11d). In the upper part of the images, the concentration of sea ice was about 100% from February to April and remained unchanged, whereas in May the situation markedly changed and zones with a lower concentration appeared. According to the images, it can be also assumed, that the blue area may be identified as coastal polynya, it becomes slightly wider during the presented period, and reaches its size peak in late May(Figure 11d).

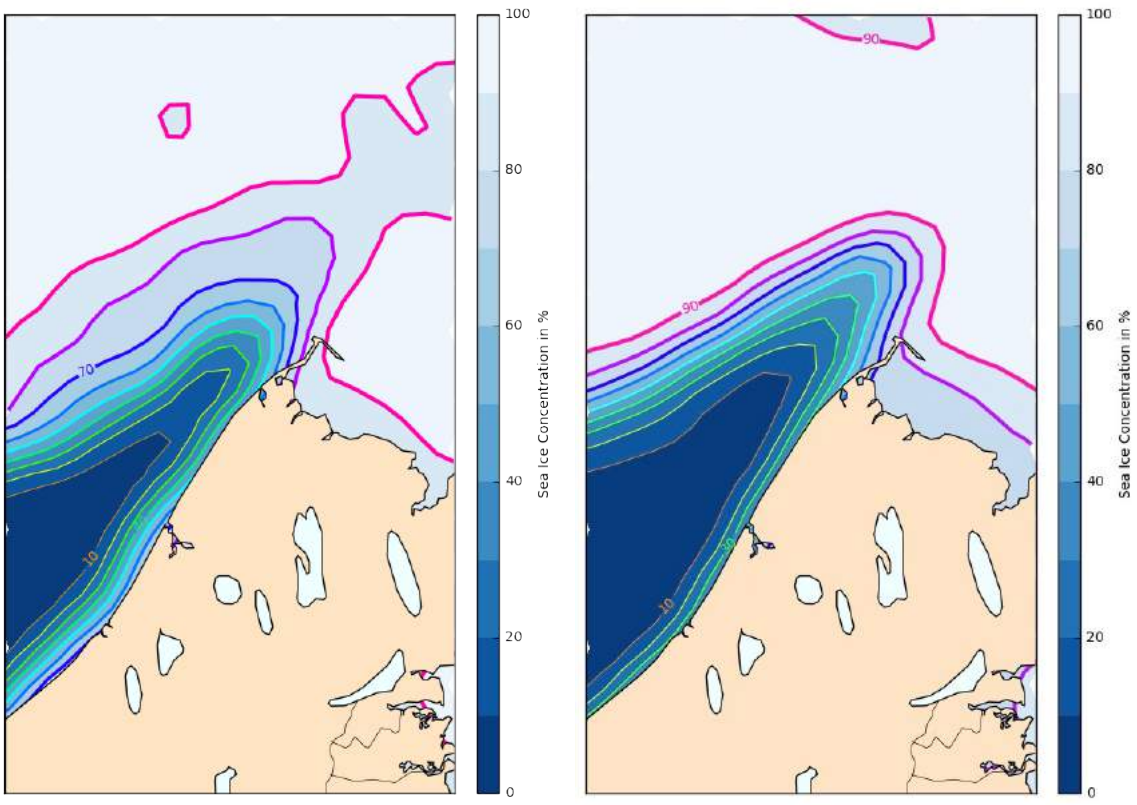

(a) 02/06/2016

(b) 03/10/2016

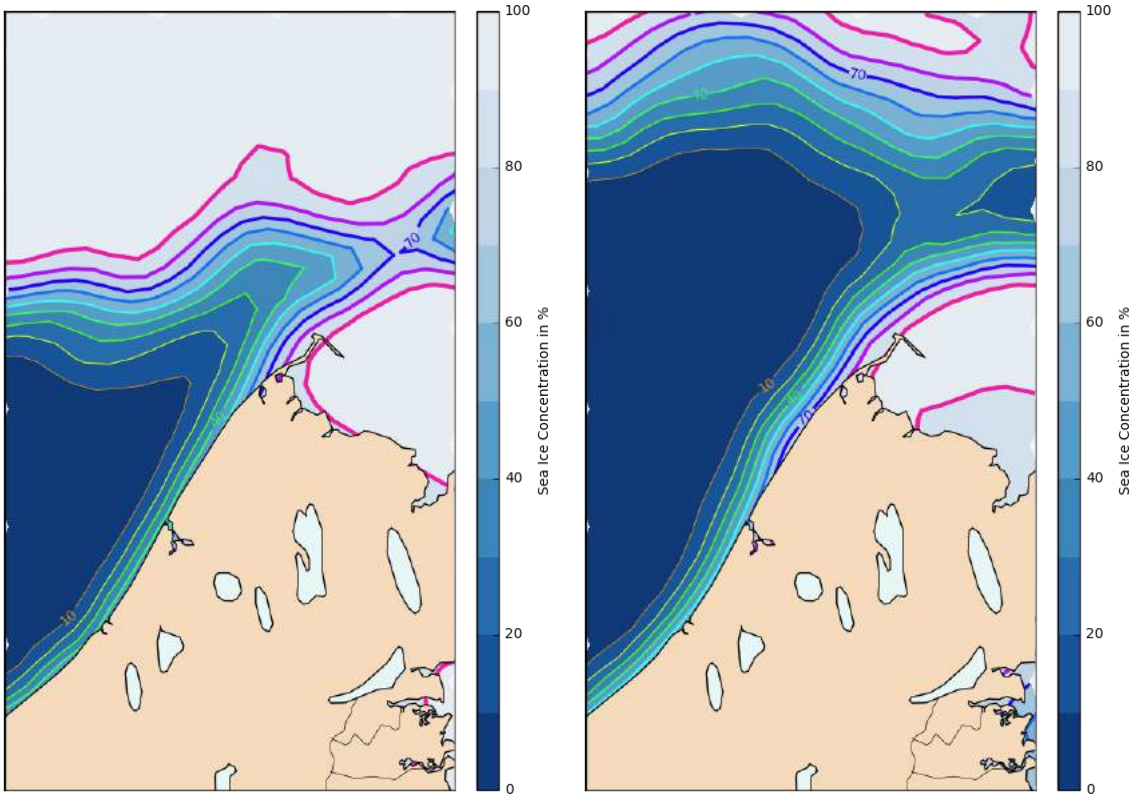

(c) 04/12/2016

(d) 05/26/2016

Figure 11: Sea ice conditions, including sea ice concentration in % with isolines around selected test site near Barrow, Alaska, obtained from AMSR2 radar, for the chosen study period.

8.2 InSAR method application

This section demonstrates the application of the InSAR method for several purposes, including drift of sea ice and fast ice detection. The received data is in interval from February 2016 till May 2016 and consists of 10 datasets, including coherence, backscatter and phase images, metadata and interferogram.

Figure 12 demonstrates several images, including interferometric phase difference, backscatter and coastal radar intensity, for February 06, 2016. On the demonstrated images the fast ice zone can be recognized with difficulties. The backscatter image exhibits no clear features which could allow to identify stationary types of ice or drift ice and separate them one from another.

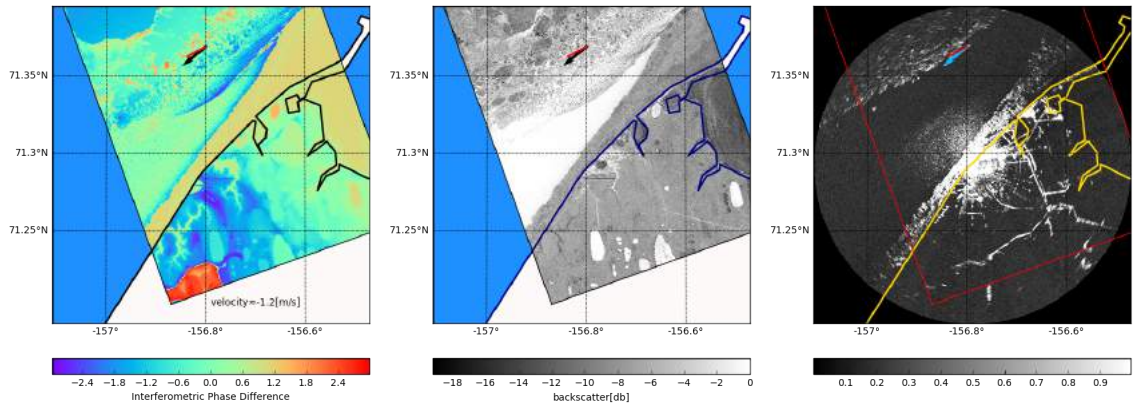

Figure 12: Interferometric phase difference (left) and backscatter image (middle), obtained from the TanDEM-X mission and coastal radar image (right), near supersite Pt. Barrow, Alaska. The arrow indicates the vector derived by manual drift calculation of particular ice formation from the coastal radar image and the red line denotes the LOS direction of this vector with approximate value of LOS velocity component. The acquisition time of the TanDEM-X images: 03:20 and coastal radar image: 03:07, for February 06, 2016.

The vectors were obtained for the coastal radar images by manual sea ice drift. Figure 12 helps to find out what particular sea ice formations were tracked and compare their location with satellite images. The applying of different data helps to find an approximate location of the landfast zone for further calculations and method improvements.

8.2.1 Offset estimation

The interferometric phase image (Figure 12) from the previous section, clearly shows, that the fast ice zone near the coast has homogeneous color field. Since the interferometric phase difference and radial velocity are linearly connected, it is obvious that the fast ice should have zero phase/velocity values, so we can assume that each phase image has particular offset value, which was necessary to be found for the purposes related to the fast ice detection. The zero phase may be selected in the area, at the sea surface level, where is no movement, in our case this is fast ice zone. Table 6 demonstrates the offset values for all examples, which have clearly visible fast ice zone.

Table 6: Phase offsets for each dataset which had fast ice zone

Acquisition date	**Offset Value**
February 06, 2016	1.125
February 17, 2016	-2.106
February 28, 2016	-2.210
March 10, 2016	1.034
March 21, 2016	-1.773
April 12, 2016	2.153
April 23, 2016	2.051
May 04, 2016	-1.253

Figure 13 shows the interferometric phase difference with fast ice area marked by white rectangle and interferometric phase difference after offset modifying, for one example, February 06, 2016. The fast ice zone can be easily distinguished by the homogeneous white color on the right image. To find the mean value of the offset, several important calculations were made. First of all, a rectangle in the fast ice zone was constructed. After that, the mean of all values falling into the range of the rectangle was calculated. As a result, this offset value was added to the interferometric phase difference. According to the Table 6 it can be said that the offset is not a constant and it has different particular value for each date.

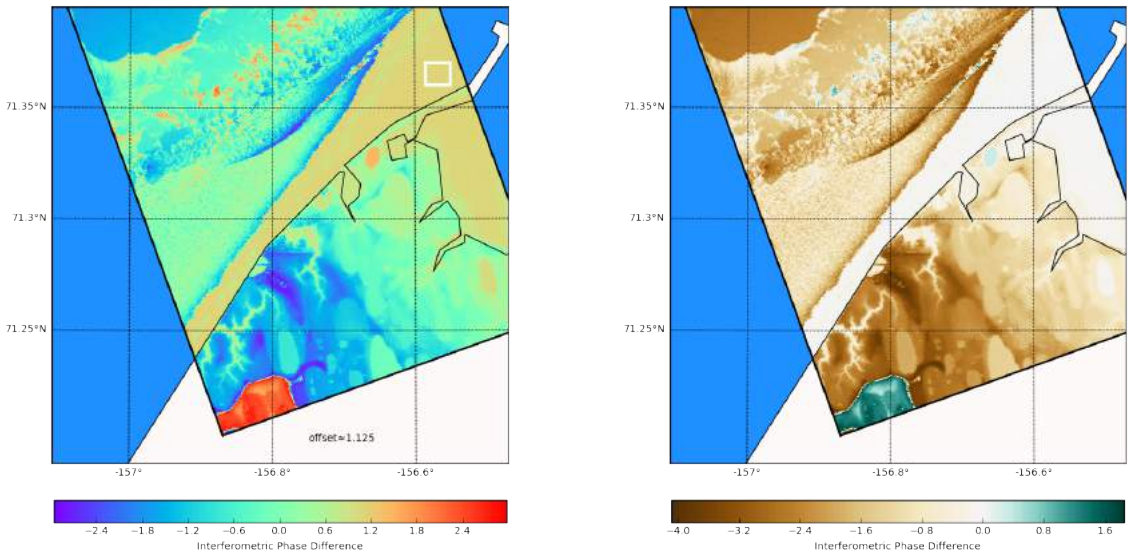

Figure 13: Interferometric phase difference with fast ice area marked by white rectangle (left) and interferometric phase difference after offset modifying (right), for February 06, 2016, near Barrow, Alaska.

8.2.2 Radial velocity maps

This section demonstrates the radial velocity maps, which are the main result of this study, for the fast ice detection and sea ice drift calculation.

Before describing the radial velocity maps, it should be clarified, that the radial or LOS velocity can involve negative and positive values depending on direction of the motion. Negative means that the object is moving towards the radar, whilst positive means the object is moving away from the radar.

The line of sight or radial velocity was calculated by dint of interferometric phase difference after the Equation 8. All the parameters presented in the equation are described in the previous sections.

Figure 14 illustrates the radial velocity with isolines of sea ice concentration and coastline (right), interferometric phase difference (left top) and zoomed radial velocity (left bottom), for February 06, 2016, near Barrow, Alaska. The fast ice zone can be easily identified by the homogeneous field of zero velocity near the coastline (white color) and clearly separated from the drift ice and open water areas. Radial velocity maps shows the sea ice moves in different directions and with different velocities. The sea ice formations which are moving towards the radar reach the velocity up to -0.2 m/s (blue area on the top of the right figure). The field of large ice floes, which is moving away from the radar with the velocities in range from 0.16

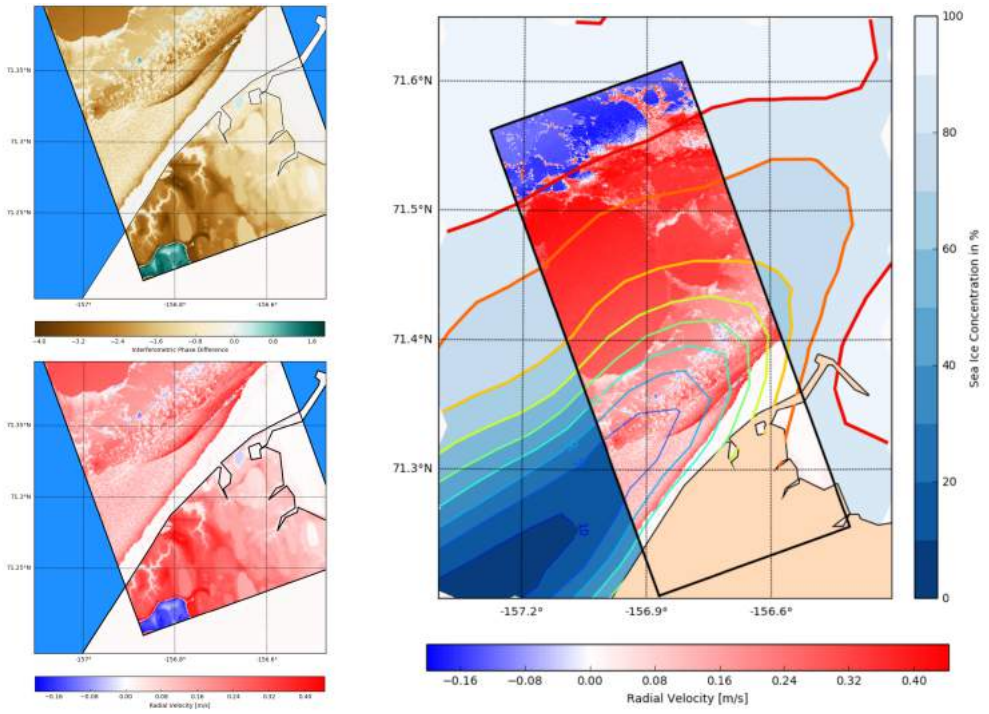

Figure 14: Radial velocity map with isolines of sea ice concentration and coastline (right), interferometric phase difference (left top) and zoomed radial velocity map for better fast ice zone detection (left bottom), for February 06, 2016, near Barrow, Alaska.

m/s to 0.45 m/s (red color on the right figure), can be also identified on the map. Zoomed radial velocity image (left bottom) shows that the sea ice near the fast ice zone moves away from the radar with lower velocity values up to 0.3 m/s.

Figure 15 and Figure 16 demonstrates the radial velocity maps for all period of observations, starting from February 06, 2016 till May 04, 2016. All the illustrated examples have different ice conditions, different ice drift velocities, which reach up to 1 m/s, but one feature remains practically unchanged - fast ice zone which can be clearly identified by the homogeneous field of zero velocity, near the coastline and separated from the drift ice zones and open water areas. This fast ice zone has a white color on all the constructed images.

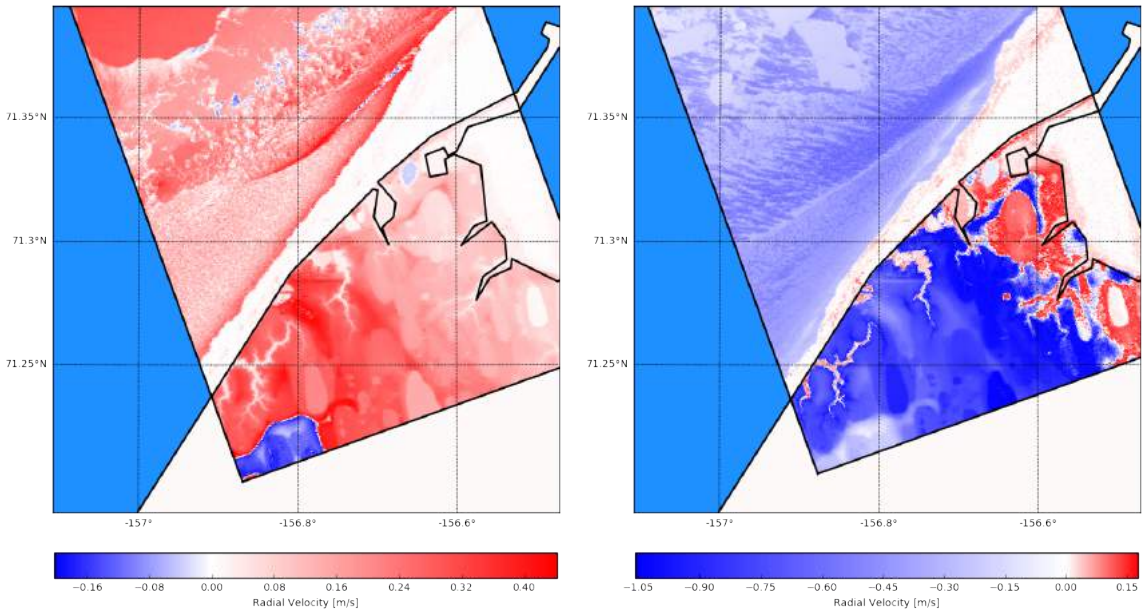

(a) February 06, 2016

(b) February 17, 2016

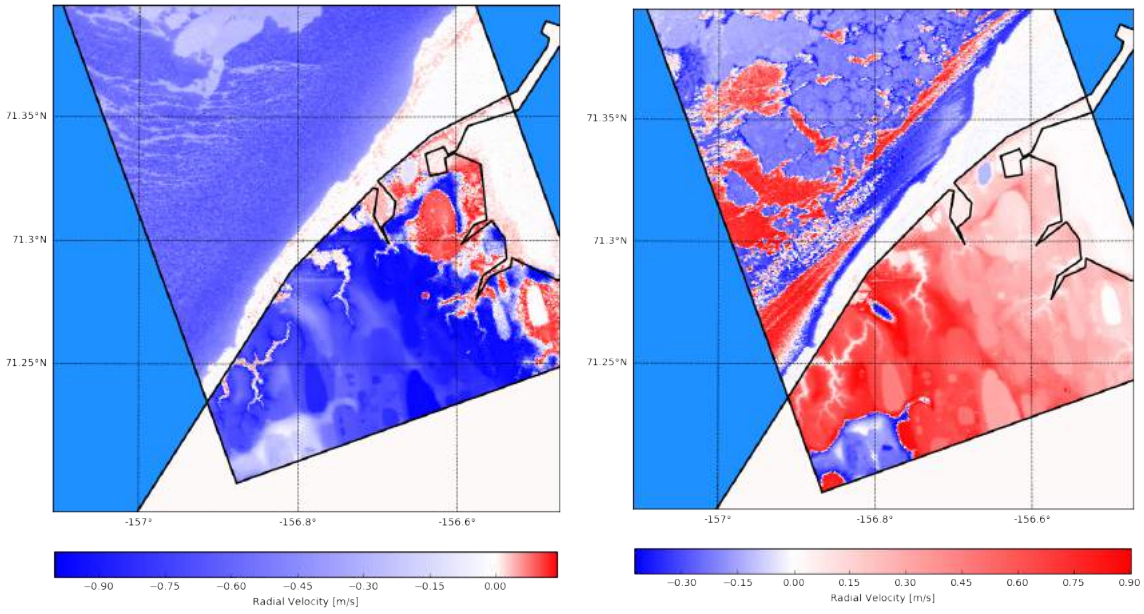

(c) February 28, 2016

(d) March 10, 2016

Figure 15: Radial velocity maps.

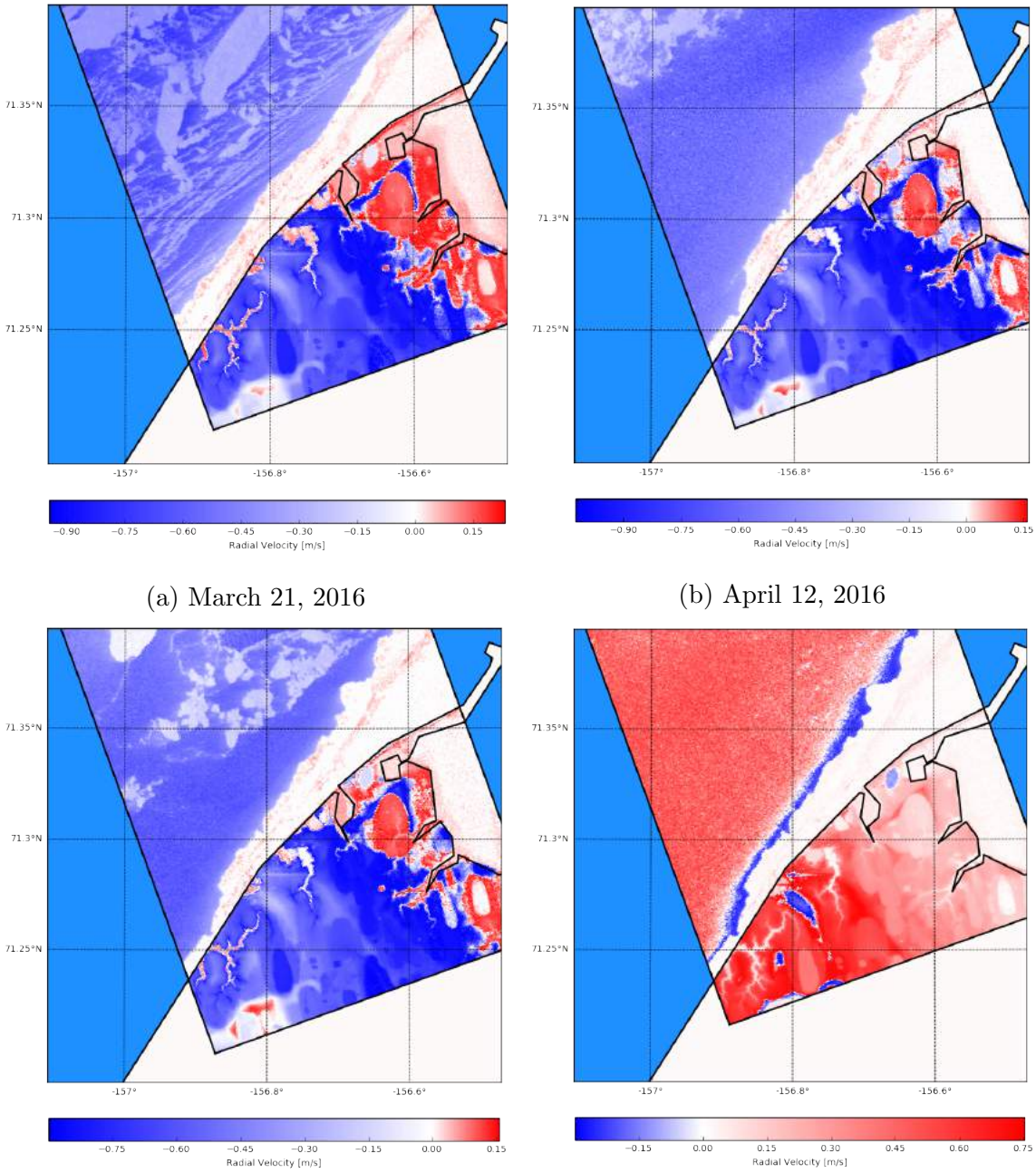

(a) March 21, 2016

(b) April 12, 2016

(c) April 23, 2016

(d) May 04, 2016

Figure 16: Radial velocity maps.

8.3 Validation of InSAR method

Two main goals of this study are fast ice detection and sea ice motion calculation. The potential of fast ice detection is evident and can be discussed with the phase/velocity images without further geocoding and validation. However, for the second purpose, sea ice motion calculation, subsequent verification is necessary.

This section demonstrates the empirical comparison of LOS velocities from InSAR and coastal marine radar. As it was already mentioned, for the validation of the InSAR method, coastal radar data were used, including images and vector velocity values. Table 7 shows the list of main values which are used for the validation of sea ice motion, including mean LOS velocity components from coastal radar vector tracking and InSAR method with additional wind speed values. Wind speed was received from NOAA [21] and was measured in meters/second.

Table 7: Main values obtained for validation, including several mean components, such as InSAR and coastal radar vectors with acquisition date and additional wind speed values.

Acquisition date	**Mean Velocity [m/s]**		
	Radar LOS	**InSAR LOS**	**Wind**
February 06, 2016	-1.21	0.09	6.87
February 17, 2016	-0.52	-0.23	10.51
February 28, 2016	-1.42	-0.56	11.32
March 10, 2016	-0.91	0.38	7.53
March 21, 2016	-0.49	-0.54	7.89
April 12, 2016	-0.31	-0.58	10.03
April 23, 2016	-0.69	-0.57	7.36

Figure 17a demonstrates satellite and coastal radar image scenes with all the used vectors, near selected test site area. According to the image, the satellite scene is inclined relative to the coastal radar scene, which creates a geometric problem that needs to be solved, for a careful comparison of two datasets. In order to compare the values of the radial velocity components (VVC) of the coastal radar and the values of the InSAR radial velocity (IRV) it is mandatory to recalculate all the images and vectors to common coordinate system and also solve the problem of inclination of satellite image scene.

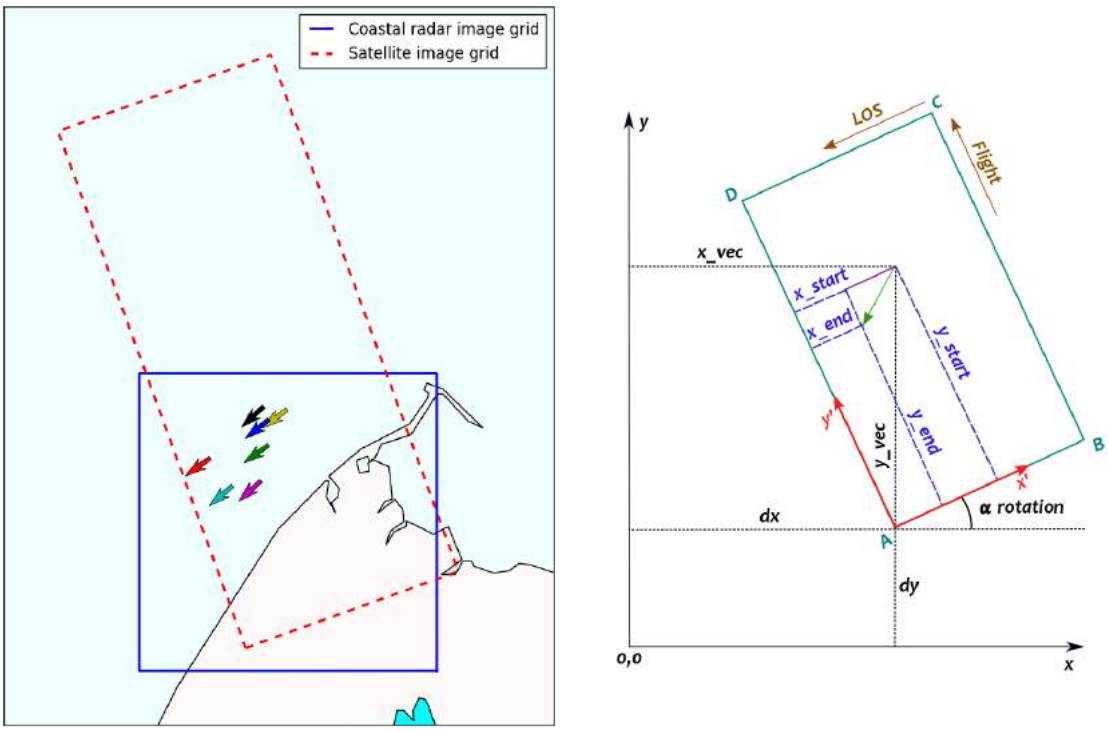

(a) Vectors location

(b) Geometrical sketch

Figure 17: Satellite and coastal radar image scenes with all vectors used for the validation (left) and geometrical sketch (right).

Figure 17b illustrates graphically the main idea and solution of the geometrical problem. The sketch demonstrates the angle of the scene related to the initial coordinate system, as well as the idea of recalculating the point coordinates from one system to another, that is offset and rotated in relation to the first one.

After all the values are transferred to the new coordinate system, it is necessary to calculate the VVC and IRV for the same areas, as well as calculate the mean value for every example to eventually get one point for each date. The next step after the points obtaining is comparison of the values, by dint of linear regression, to obtain important statistical parameters.

Figure 18 demostrates scatter plot and linear regression of VVC and IRV. Table 8 demonstrates the main statistical parameters of VVC and IRV comparison. According to the Table 8 the mean value for the VVC is equal to: -0.79 and for IRV: -0.29. The standard error is equal to -0.4. The Pearson correlation coefficient is approximately equal to -0.32, which means that between two radial velocities there is a weak negative correlation. Unfortunately, the data sample was not very wide, which may lead to unconfident statistical values for the description of the results.

There may be several reasons for such a weak correlation of radial velocities, for instance, phase offset, inaccuracies in manual sea ice drift, or incorrect coincidence in time between two datasets. Since sea ice moves with a velocities of about 0.3 m/s, it is fairly difficult to trace the same ice formations using different types of information (satellite and coastal radar).

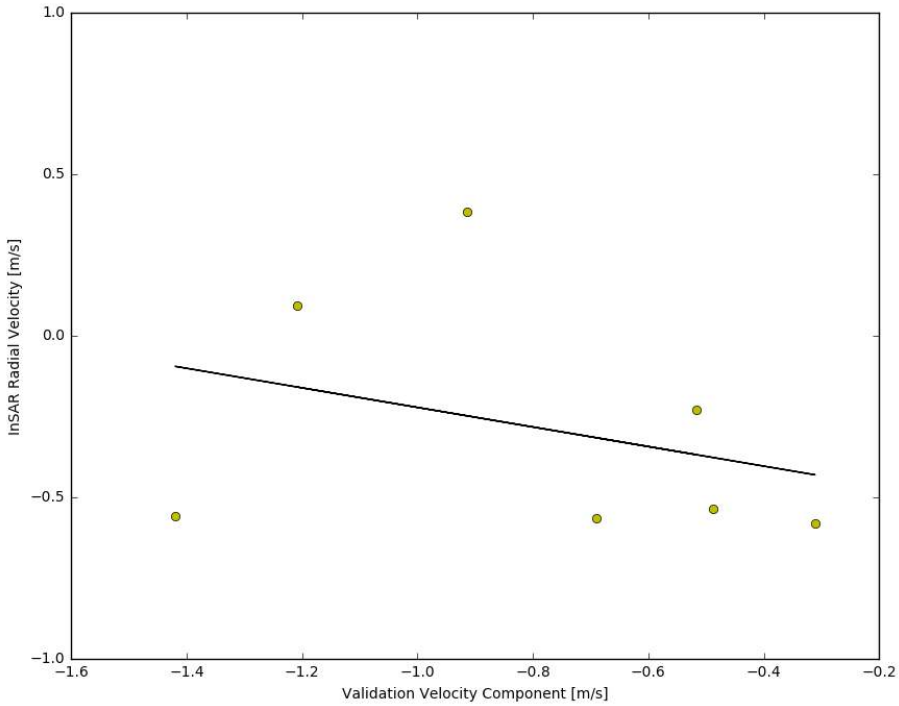

Figure 18: Scatter plot and linear regression of VVC and IRV.

Table 8: Statistical values obtained from the comparison of VVC and IRV

	Statistical Parameters
Slope	-0.30
Intercept	-0.53
r_value	-0.32
std_err	-0.40
	Mean Value
VVC	-0.79
IRV	-0.29
	Standard Deviation Value
VVC	-0.38
IRV	-0.36

9 Discussion

This section, demonstrates the discussion of several InSAR method applications, including fast ice detection and radial velocity calculation. It should be noted that no peer-reviewed publications exist concerning the use of SP-InSAR for sea ice applications. The reason for this could be the limited access to TanDEM-X data. This work is the first InSAR ATI study for computing the sea ice motion and fast ice detection by dint of interferometric phase difference. However, there were already some particular studies that used the same method and the same radars, but for other purposes, for example, ocean surface observations [29], calculation of surface current fields, by dint of doppler centroid analysis [23], etc [24] [30]. The values from the ocean currents theory not ideally suited for the sea ice velocity calculation and fast ice detection requirements, therefore, it became necessary to develop a sea ice theory for calculating the sea ice motion magnitude and direction.

It is worth noting again, that only the radial component of the surface velocity was calculated. The radial velocity can assume positive and negative values depending on the direction of the movement (towards or away from the radar), however, if the object moves perpendicular (sideways) to the trajectory of the survey this will be regarded as zero motion.

The discussion section should be divided into two main parts: fast ice detection and sea ice motion calculation, since these are the several principal goals of the work and they imply a different result. The results are really encouraging, particularly those for fast ice purposes.

9.0.1 Fast ice detection

The first step in working with an interferogram for fast ice detection, was raster generalization, which was applied, in order to remove small unnecessary isolated regions from the interferometric phase difference image, for better identification of landfast ice zones.

As it was already described earlier, the main problem, which prevented the allocation of zero fast ice zones, was the phase offset which is clearly visible on the interferogram images. So, the offset calculation is the second processing step. The interferometric phase difference is linearly related to the radial component of the velocity, measured by the radar, which implies that the fast ice on the phase/velocity

images should be a priori equal to zero. To find the offset, some scientific assumptions were added to the Equation 6. First assumption implies no changes in surface topography in time. Second assumption means that the fast ice has the same thickness as the drift ice. That allows to choose the offset in the way the fast ice in the phase image has a $\Delta\phi$ of about zero. This allows to skip all the cases without fast ice zone near the coastline area. In order to add a correction for the interferogram image, the mean offset value was calculated for each image. After the correction, the fast ice zones can be easily identified by the homogeneous field of zero velocity and clearly distinguished from the drift sea ice types, open water areas and coastline.

Comparing InSAR method for fast ice detection requirements with other methods which can be used for the same purposes, it can be truly said, that the main advantage of SP-InSAR is the possibility to derive the instantaneous motion field and thus the fast ice zone with single overpasses. These results clearly demonstrate the feasibility of fast ice detection by dint of InSAR method, which would be really useful for the scientific and commercial needs.

9.0.2 Sea ice LOS motion

An EOWEB [8] archive search resulted more than 200 TanDEM CoSSC images available since 2011, for the selected test site which is also monitored by the coastal marine radar. This TanDEM CoSSC data together with the coastal radar data generate a good basis for validation of sea ice motion from SP-InSAR. It is necessary to note that this empirical comparison would be the first based on a extensive dataset for a wide range of sea ice conditions and for different along-track baselines with theoretical analysis of SP-InSAR imaging mechanism for scenes mixed with sea ice and ice-free ocean. This study has the potential to strongly improve available knowledge and understanding of the possibilities for sea ice motion retrieval from SP-InSAR.

For the calculation of the radial velocity by dint of interferometric phase difference, the Equation 8 was used. This equation is transformation of another Equation 7 obtained from the Suchand et al. (2010) [30]. Some of the parameters used in the equation are constant, for instance sensor velocity U_s for TerraSAR-X is approximately equal to 7.6 km/s (7,600 m/s) and radar wavelength λ for X-band is equal to 0.03 m. However, there are such parameters that are different for each dataset,

including along-track baseline B_{al} and interferometric phase difference $\Delta\phi$.

As it known, sea ice motion can reach the velocity up to 1 m/s. The maps of the radial velocity distribution show credible values of velocity in range of 0 to 1 m/s. However, the subsequent comparison of the vectors from the coastal radar images and the values obtained from the satellite images did not yield any strong correlation. The Pearson correlation coefficient is equal to -0.32, which means that between two radial velocities there is a weak negative correlation. That indicates the negative result for the velocity validation and the need for further improvement and verification of the method in terms of calculating the velocity of sea ice. Perhaps, for subsequent validation it will be reasonable to use the wider sample of points.

Table 8 illustrates the standard deviation that describes quantify the amount of variation or dispersion of a set of values is equal 0.38 for VVC and 0.36 for IRV. Large uncertainty of data can be the consequence of the unknown bias for each phase image. Another possible reason of the uncertainty could be the effect of wind/waves in the mixed open water/sea-ice covered area.

10 Conclusions

The fast ice detection and calculation of the velocity and direction of the sea ice drift, near Barrow, Alaska, was investigated for the period from early February, 2016 until late May, 2016. Results of the work with interferometric phase difference, namely radial velocity maps, demonstrates that the fast ice on the satellite images can be easily identified by the homogeneous fields of zero velocity and distinguish from the drift ice and open water areas. However, sea ice motion calculations show a negative result, which was obtained after comparing the radial velocities from the coastal radar and satellite data.

From the manipulations with data, it became clear that the interferometric phase difference is linearly related to the radial velocity. Unfortunately, the accuracy of estimating the velocity of sea ice and surface currents appears to be not very accurate. Errors can be directly related to the fact that the interferometric phase difference contains several types of information, including the surface motion, topography of the underlying surface and noise (Equation 6). That is why we can not expect correct absolute values but only differences, which is sufficient to separate drift and stationary types of ice on the underlying surface.

If to compare the InSAR method for the purposes of fast ice detection and sea ice motion calculation with other automatic methods, such as: polynomial, cross-correlation, hybrid or other methods, it can be said that the main difference and at the same time the primary advantage is that a pair of images is obtained almost simultaneously (the interval is less than a second, approximately milliseconds), this in turn allows to conduct the operational sea ice monitoring. This is quite important advantage for navigation on the main polar routes (prevent accidents with dangerous ice phenomena).

Acknowledgements

I would like to acknowledge everyone who played a role in my master thesis. Foremost, my supervisors, Prof. Dr. Lars Kaleschke and Dr. Vladimir Volkov who guided my work and gave useful scientific advices. Moreover, I would like to express my gratitude to Saint-Petersburg State University, Hamburg University, Nansen International Environmental and Remote Sensing Centre and POMOR master's program for the great support. And the last but not the least, I would like to thank my colleagues who also advised and helped me.

The copyright for TerraSAR-X and TanDEM-X data used in this paper is with the German Aerospace Center (DLR). TanDEM-X data were obtained through TanDEM-X science project ATI_DGLAC7109 (Principal Investigator: L. Kaleschke).

References

[1] D. E. Alsdorf and L. C. Smith. Interferometric SAR observations of ice topography and velocity changes related to the 1996, Gjalp subglacial eruption, Iceland. *Remote Sensing*, 20(15-16):3031–3050, 1999. doi: http://dx.doi.org/10.1080/014311699211606.

[2] R. Bamler and P. Hartl. Synthetic aperture radar interferometry. *Inverse Problems*, 14(4), 1998.

[3] L. Bickel. Sar Image Effects on Coherence and Coherence Estimation. *Sandia Report*, 2014. doi: 10.2172/1147517.

[4] A. V. Bushuyev. Sea Ice Nomenclature. Technical Report WMO. 1968.

[5] W. Dierking. Sea ice monitoring by synthetic aperture radar. *Oceanography*, 26(2):100–111, 2013. doi: https://doi.org/10.5670/oceanog.2013.33.

[6] W. Dierking, O. Lang, and T. Busche. Sea ice local surface topography from single-pass satellite InSAR measurements: a feasibility study. *The Cryosphere Discuss*, 2017. doi: 10.5194/tc-2017-40.

[7] DLR. Tandem-x Mission. http://www.dlr.de/dlr/en.

[8] EOWEB. Earth Observation Data. https://centaurus.caf.dlr.de:8443/.

[9] ESA. Radar and SAR Glossary. https://earth.esa.int/handbooks/asar/CNTR5-2.html.

[10] EUMETSAT. Ocean and Sea Ice SAF. http://osisaf.met.no/p/ice/.

[11] R. Goldstein, T. Barnett, and H. Zebker. Remote Sensing of Ocean Currents. *Science*, 246(4935):1282–1285, 1989. doi: 10.1126/science.246.4935.1282.

[12] R. Goldstein, C. Werner, and H. Zebker. Satellite radar interferometry: Two-dimensional phase unwrapping. *Radio Science*, 23(4):713–720, 1988. doi: 10.1029/RS023i004p00713.

[13] N. E. Hughes, J. P. Wilkinson, and P. Wadhams. Multi-satellite sensor analysis of fast-ice development in the Norske Øer Ice Barrier, northeast Greenland. *Annals of Glaciology*, 52(57):151–160, 2011. doi: 10.3189/172756411795931633.

[14] L. Kaleschke and W. Dierking. Study of Potential Application for Future Single-pass Interferometric SAR instruments, Sea Ice. pages 63–78, 2014.

[15] A. Klene, K. Hinkel, F. Nelson, and J. Bell. The urban heat island in winter at Barrow, Alaska. 23(15), 2003. doi: 10.1002/joc.971.

[16] G. Krieger, I. Hajnsek, K. Papathanassiou, M. Younis, and A. Moreira. Interferometric Synthetic Aperture Radar (SAR) Missions Employing Formation Flying. *IEEE*, 98(5):816–843, 2010. doi: 10.1109/JPROC.2009.2038948.

[17] P. Lopez-Dekker, G. Krieger, and A. Moreira. Multistatic Radar Systems. *Distributed Space Missions for Earth System Monitoring Space Technology*, 31, 2013. doi: 10.1007/978-1-4614-4541-8.

[18] A. Mahoney, H. Eicken, Y. Fukamachi, K. Ohshima, D. Simizu, C. Kambhamettu, M. Rohith, S. Hendricks, and J. Jones. Taking a look at both sides of the ice: comparison of ice thickness and drift speed as observed from moored, airborne and shore-based instruments near Barrow, Alaska. *Annals of Glaciology*, 56(69):363–372, 2015. doi: 10.3189/2015AoG69A565.

[19] F. J. Meyer, A. R. Mahoney, H. Eicken, C. L. Denny, H. C. Druckenmiller, and S. Hendricks. Mapping arctic landfast ice extent using L-band synthetic aperture radar interferometry. *Remote Sensing of Environment*, 115(12):3029–3043, 2011. doi: https://doi.org/10.1016/j.rse.2011.06.006.

[20] A. Moreira, P. Prats-Iraola, M. Younis, G. Krieger, I. Hajnsek, and P. Papathanassiou. DLR, A Tutorial on Synthetic Aperture Radar. *IEEE Geoscience and Remote Sensing Magazine*, 1(1):6–43, 2013. doi: 10.1109/MGRS.2013.2248301.

[21] NOAA. Earth System Research Laboratory. https://www.esrl.noaa.gov/gmd/dv/data.

[22] R. Romeiser, H. Breit, M. Eineder, H. Runge, and P. Flament. Current Measurements by SAR Along-Track Interferometry From a Space Shuttle. *IEEE Transactions on Geoscience and Remote Sensing*, 43(10):2315–2324, 2005. doi: 10.1109/TGRS.2005.856116.

[23] R. Romeiser, H. Runge, S. Suchandt, R. Kahle, C. Rossi, and P. S. Bell. Quality Assessment of Surface Current Fields From TerraSAR-X and TanDEM-X Along-Track Interferometry and Doppler Centroid Analysis. *IEEE Transactions on Geoscience and Remote Sensing*, 52(5):2759–2772, 2014. doi: 10.1109/TGRS.2013.2265659.

[24] R. Romeiser and D. R. Thompson. Numerical Study on the Along-Track Interferometric Radar Imaging Mechanism of Oceanic Surface Currents. *IEEE Transactions on Geoscience and Remote Sensing*, 38(1):446–458, 2000. doi: 10.1109/36.823940.

[25] P. A. Rosen, S. Hensley, I. R. Joughin, F. K. Li, S. N. Madsen, E. Rodriguez, and R. M. Goldstein. Synthetic Aperture Radar Interferometry. *Proceedings of the IEEE*, 88(3):333–382, 2000. doi: 10.1109/5.838084.

[26] S. Sandven and O. Johannessen. Sea Ice Monitoring by Remote Sensing. *Encyclopedia of Analytical Chemistry*, 2006. doi: 10.1002/9780470027318.a2320.

[27] M. Shokr and N. Sinha. Sea Ice. Physics and Remote Sensing. 2015. doi: 10.1002/9781119028000.

[28] U. Steinbrecher, M. Zink, A. Moreira, M. Bachmann, J. Boer, D. Shulze, and G. Krieger. Remote Sensing and Spatial Information Sciences, TanDEM-X mission: overview, status and outlook. *International Archives of the Photogrammetry*, XL-1-W1:327–331, 2013. doi: https://doi.org/10.5194/isprsarchives-XL-1-W1-327-2013.

[29] S. Suchandt and H. Runge. Ocean Surface Observations Using the TanDEM-X Satellite Formation. *IEEE Journal of selected topics in applied Earth observations and Remote Sensing*, 8(11):5096–5105, 2015. doi: 10.1109/JSTARS.2015.2446893.

[30] S. Suchandt, H. Runge, H.Breit, U.Steinbrecher, A. Kotenkov, and U. Balss. Automatic Extraction of Traffic Flows Using TerraSAR-X Along-Track Interferometry. *IEEE Transactions on Geoscience and Remote Sensing*, 48(2):807–819, 2010. doi: 10.1109/TGRS.2009.2037919.

[31] UAF. Barrow Sea Ice Radar. http://seaice.alaska.edu/gi/observatories/barrow_radar.

[32] F. T. Ulaby and D. G. Long. Microwave Radar and Radiometric Remote Sensing, Interferometric Synthetic-Aperture Radar. pages 743–781, 2014.

[33] L. Zhong and L. Zhang. Frontiers of Radar Remote Sensing. *Photogrammetric Engineering and Remote Sensing*, pages 5–13, 2014.

Statement on the thesis originality

Herewith I, Khachatrian Eduard, declare that I wrote the thesis independently and did not use any other resources than those named in the references, and, in particular, did not use any internet resources except for those named in the references. The master thesis has not been used previously as part of an examination. The master thesis has not been previously published.